

See discussions, stats, and author profiles for this publication at: <https://www.researchgate.net/publication/231700828>

Melt Structure and Dynamics of Unentangled Polyethylene Rings: Rouse Theory, Atomistic Molecular Dynamics Simulation, and Comparison with the Linear Analogues

ARTICLE *in* MACROMOLECULES · NOVEMBER 2010

Impact Factor: 5.8 · DOI: 10.1021/ma1017555

CITATIONS

34

READS

29

5 AUTHORS, INCLUDING:



Nikolaos Stratikis

University of Patras

2 PUBLICATIONS 34 CITATIONS

[SEE PROFILE](#)



Pavlos Stephanou

ETH Zurich

25 PUBLICATIONS 156 CITATIONS

[SEE PROFILE](#)

Melt Structure and Dynamics of Unentangled Polyethylene Rings: Rouse Theory, Atomistic Molecular Dynamics Simulation, and Comparison with the Linear Analogues

Georgia Tsolou, Nikos Stratikis, Chunggi Baig,* Pavlos S. Stephanou, and
Vlasis G. Mavrntzas*

Department of Chemical Engineering, University of Patras & FORTH-ICE/HT, Patras, GR 26504, Greece

Received August 5, 2010; Revised Manuscript Received October 18, 2010

ABSTRACT: Atomistic configurations of model unentangled ring polyethylene (PE) melts ranging in chain length from C_{24} up to C_{400} have been subjected to detailed molecular dynamics (MD) simulations in the isothermal–isobaric statistical ensemble at temperature $T = 450$ K and $P = 1$ atm. Strictly monodisperse samples were employed in all cases. We present and discuss in detail simulation results for a variety of structural, thermodynamic, conformational and dynamic properties of these systems, and their variation with chain length. Among others, these include the mean chain radius of gyration, the pair correlation function, the intrinsic molecular shape, the local dynamics, the segmental mean square displacement (msd), the chain center-of-mass self-diffusion coefficient D_G , the chain terminal relaxation time τ_d , the characteristic spectrum of the Rouse relaxation times τ_p , and the dynamic structure factor $S(q,t)$. In all cases, the results are compared against the corresponding data from simulations with linear PE melts of the same chain length (the linear analogues) and the predictions of the Rouse theory for polymer rings which we derive here in its entirety. The Rouse theory is found to provide a satisfactory description of the simulation findings, especially for rings with chain length between C_{50} and C_{170} . An important finding of our work (from the observed dependence of D_G , τ_p , ζ , and η_0 on chain length N) is that PE ring melts follow approximately Rouse-like dynamics even when their chain length is as long as C_{400} ; this is more than twice the characteristic crossover chain length ($\sim C_{156}$) marking the passage from Rouse to reptation dynamics for the corresponding linear PE melts. In a second step, and by mapping the simulation data onto the Rouse model, we have managed to extract the friction coefficient ζ and the zero-shear rate viscosity η_0 of the simulated ring melts. Overall, and in agreement with previous theoretical and experimental studies, our simulation results support that the structure of ring polymers in the melt is more compact than that of their linear analogues due to their nonconcatenated configurations. Additional results for the intermolecular mer–mer and center-of-mass pair correlation functions confirm that the effective correlation hole effect is more pronounced in melts of rings than in melts of linear chains.

1. Introduction

Polymeric materials exhibit a variety of fascinating phenomena which in their majority are manifestations of the huge number of degrees of freedom underlying their macromolecular structure. As a result, property–structure relationships in polymeric liquids extend over a broad spectrum of characteristic length and time scales which in turn depends critically on the exact chemical composition and molecular architecture of the constituent chains.^{1–4} To understand, in particular, the rheological behavior of polymeric liquids, one should understand the interplay between the large number of internal degrees of freedom possessed by a chain and the macroscopically applied flow, an extremely complicated problem which is also reflected on the many different material functions that one should measure for a given polymer in order to classify its rheological behavior. How these material functions can then be compiled in terms of a few molecular parameters by grouping polymers together is still not well understood. We can mention, for example, the totally different rheological properties exhibited by polymers that bear long- or short-branches along

their main chain backbone, by polymers with a dendritic or hyperbranched structure, by star polymers, etc.^{5–7} In this rather wide range of molecular architectures for polymers, the best understood today from a rheological point of view are the families of linear and long-chain branched ones. Our knowledge here comes mainly from the reptation theory^{8–10} which accounts in a very efficient way for the restrictions in chain motion imposed by the topological interactions underlying melt structure in high molecular weight (MW) polymers. In reptation, one can describe chain motion in a melt of entangled chains by considering it as a one-dimensional diffusive motion inside a curvilinear tube, which of course should be regarded in a mean-field sense.^{8–10} In the case of linear polymers, chain dynamics is therefore governed by the overall chain reptation plus a couple of other relaxation mechanisms associated with effects widely known today as contour length fluctuations (CLFs) and constraint release (CR). For branched polymers, on the other hand, additional deep CLFs of the dangling arms (branches) all the way down to the respective branch point should be taken into account for a quantitative description of their dynamics.¹¹ Owing to numerous experimental and theoretical efforts in the last years,^{9,11–13} our understanding of the melt rheology of these systems (linear and long-chain branched polymers including stars) has expanded considerably.

*Authors to whom correspondence should be addressed. (C.B.) E-mail: cbaig@iceht.forth.gr. Telephone: +30-2610-965219. Fax: +30-2610-965223. (V.G.M.) E-mail: vlasis@chemeng.upatras.gr. Telephone: +30-2610-997398. Fax: +30-2610-965223.

Reptation applies straightforwardly to polymers with chain ends. But what about if the molecule does not possess any chain ends? A model system which falls in this category is that of polymer rings.¹⁴ For a ring chain, the standard reptation theory is not directly of relevance because the complete absence of chain ends invalidates relaxation mechanisms such as curvilinear chain reptation inside a cylindrical tube and/or CLFs. As analyzed by Klein,¹⁵ even if one is tempted to envisage reptation in rings by assuming a linear (nonramified) double strand conformation for a ring molecule, such a conformation would be statistically improbable since it is extremely unfavorable entropically; besides, a reptation-type of motion for a double linear strand would require a perfect dynamical correlation of the two strands for a certain period of time, which is again quite improbable to be realized in practical systems.

Historically, the first description of ring polymers was set forth by Kramers,¹⁶ who calculated that, in the absence of excluded-volume and hydrodynamic interactions, the mean-square radius of gyration $\langle R_g^2 \rangle$ and the intrinsic viscosity of a ring polymer in a dilute solution should be half those of the corresponding linear polymer of the same molecular weight (the linear analogue). A detailed treatment of the structural and dynamic properties of ring chain systems and a comparison with linear analogues was later offered by Zimm and Stockmayer¹⁷ and by Casassa¹⁸ who further included a description of their thermodynamic behavior. Ring polymer dynamics in a dilute solution has been addressed also by Bloomfield and Zimm¹⁹ and independently by Fukatsu and Kurata²⁰ through an extension of the original Rouse²¹ and Zimm²² theories. A more detailed theoretical account of the Rouse model for ring polymers has been reported by Watanabe et al.²³ However, a comprehensive analysis of the full theory, together with a complete appreciation of its predictions for a variety of rheological properties for rings, is still lacking; it is one of the aims of this paper to fill this gap by deriving and presenting the theory in its entirety.

The structural and rheological properties of ring polymer melts are particularly intriguing to the community of polymer rheologists due to their built-in molecular topology. For instance, it is generally known from experimental measurements^{24,25} and simulations^{26–33} that for ring polymer melts the scaling exponent ν in the relation $R_g \sim N^\nu$ is less than $1/2$ (the value for linear polymer melts), usually between $1/2$ and $1/3$. The effect of the intrinsic built-in ring topology has its origin on the constraint that only unknotted and unconcatenated chain configurations are allowed. From a physical viewpoint, the former restriction (unknotted structures) should cause an increase in chain dimensions (as was shown by Deutsch³⁴ for an isolated phantom ring molecule without excluded volume interactions) whereas the latter (unconcatenated conformations) should decrease the ring size. It is also a generally accepted view that a sufficiently long unknotted and unconcatenated ring molecule in a fixed network or melt should display a ramified hierarchical tree-like structure with multiple branches, the so-called lattice animal structure.^{35,36} Adopting such a picture for the dynamics of ring chains in melt has led to predictions for their rheological properties that are indeed quite different compared to those of linear systems.^{37,38}

In an effort to understand and quantify the equilibrium dynamics and rheological properties of polymer rings, numerous experimental efforts have been undertaken on ring molecules both in solution and melt.^{38–61} And although viscosity measurements on long rings in dilute solutions and on short rings in melts generally appear to support the Rouse–Zimm theory, a clear picture is still missing because in many cases different experiments lead to controversial results.^{38,40,42,44,60,61} This is especially so in the case of long rings in melt. The reason for this should be most likely sought to experimental limitations to eliminate any contamination by linear molecules. Kapnistos et al.,³⁸ for example,

found that even a tiny fraction of linear contaminants in a ring polystyrene (PS) melt can cause significant changes in its rheological properties. Despite major advances in the field, it is still a formidable task to synthesize polymer melts made up 100% by ring chains.^{38,61–63} In this regard, computer simulations can be considered as an excellent alternative because they offer the opportunity to build and then simulate well-defined model ring systems of a prescribed configuration. And this explains the large amount of simulation studies that have appeared in the past few years in the literature,^{26–34,64–75} which have provided invaluable information for a variety of ring systems (isolated rings, solutions of pure rings, melts of pure rings, binary blends of ring and linear molecules, etc.).

An advantage of molecular simulations is that they offer a means for studying separately the effect of certain factors on the structural and dynamical properties of the system. We mention, for example, the capability to study the effect of architectural restrictions (knotted versus unknotted structures, concatenated versus unconcatenated configurations, etc.), of chain stiffness, of excluded volume interactions, and many others. Thus, by using a lattice-based dynamic Monte Carlo method, the so-called bond fluctuation model (BFM), Müller et al.³⁰ have observed that an increase in the chain stiffness of a ring molecule causes a decrease in the value of the scaling exponent ν in melts (ν changes from $2/5$ for a flexible ring to $1/3$ for a semiflexible ring) and a significant decrease in the value of its center-of-mass diffusion coefficient. By using again the BFM, Brown et al.³¹ performed an interesting study of the relative effect of topological restrictions on rings either isolated or in melts: by turning on and off chain uncrossability conditions, they found that whereas the influence of topological constraints is almost negligible for an isolated ring, it can be dramatic for rings in melts; e.g., by allowing rings to cross each other in the melt, the well-known Gaussian statistics $R_g \sim N^{1/2}$ is recovered, whereas $R_g \sim N^{0.42}$ for noncrossing rings. The bond fluctuation model has also been used by Shanbhag and co-workers^{33,73–75} in an extensive study of the structural and dynamical properties of binary blends of ring and linear polymer melts. By varying the overall concentration of the system or relative fraction of linear and ring chains, these investigators^{33,73–75} were able to identify the important role of the linear molecules in the dynamics of the blend: for example, they were able to observe the formation of a percolating entangled network for long ring polymers via threading of ring molecules by linear chains even for very small volume fractions of the linear component;⁷⁴ clearly, this corroborates the arguments of Kapnistos et al.³⁸ More recently, Vettorel et al.^{64,65} have implemented an efficient on-lattice Monte Carlo model which allowed the study of the conformational and structural characteristics of long ring polymer melts: they found that the average size of a polymer ring shrinks as the chain length increases since its radius of gyration R_g scales with N as $R_g \sim N^{1/3}$ in the limit $N \rightarrow \infty$; exactly the same scaling has been reported by Suzuki et al.²⁶ on the basis of simulation data with the bond fluctuation model and a self-consistent theory for melts of polymer rings.

Clearly, molecular simulations have helped obtain invaluable information about the structural and dynamic properties of ring polymers, especially as far as their comparison with the corresponding properties of linear chains is concerned. In their majority, these simulations have been performed with coarse-grained lattice Monte Carlo algorithms, whose results are not easy to compare with experimental data in a direct way. On the other hand, it is true that atomistic MD studies of ring polymers have also been performed. We can mention, for example, the atomistic MD studies of Jang et al.⁶⁶ with dilute solutions of polyethylene (PE) rings and of Hur et al.²⁷ with melts of PE rings. To help in this direction, we present additional simulation data here for the dynamics of PE rings in their molten state from long

MD runs with a very accurate force field, together with a detailed analysis of the Rouse model for ring chains. For reasons that will become more transparent in the following sections of this paper, we have restricted this work exclusively to unentangled rings. In addition, in all cases, we directly compare against the corresponding simulation and theoretical results for linear chains. One of the most significant achievements of our work is the calculation of two important rheological properties of these systems: of the monomer friction coefficient ζ and of the zero-shear rate viscosity η_0 . A direct comparison with the corresponding data for linear analogues reveals then a wealth of interesting phenomena for the dynamics of unentangled polymer rings.

The paper is organized as follows. In section 2, we give a detailed presentation of the Rouse model for ring chains in the continuum limit; the corresponding and more rigorous discrete model is presented in the Appendix of the paper. The molecular model employed in our atomistic MD simulations and details of the ring PE systems simulated in this work are given in section 3. Our results (extracted either directly from the simulations or indirectly by properly mapping the simulation data onto the re-derived Rouse model) are presented and discussed in due detail in section 4. The paper concludes with section 5 where we summarize the major findings of this study and discuss future plans.

2. Theory

In this section, we provide a detailed analysis of the continuous Rouse model for ring polymers, which is strictly valid only when $N \rightarrow \infty$ (the corresponding analysis of the discrete model is presented in the Appendix). Our analysis refers to a melt composed of short unentangled ring molecules, where hydrodynamic interactions are assumed to be effectively screened out and no topological interactions between molecules need to be considered. To gain a deeper insight into the effect of the ring architecture on the structural and dynamical properties of these polymers, we frequently contrast the model predictions to those of the corresponding theory for linear molecules of the same chain length (the so-called “linear analogues”).

In the Rouse model, a polymer molecule is considered as a sequence of coarse-grained beads characterized by an effective hydrodynamic friction coefficient ζ that are connected by Gaussian and mass-less springs (connectors) with a modulus (or spring constant) K equal to $3k_B T/b^2$ where k_B is Boltzmann’s constant, T the temperature, and b^2 the average mean square distance between adjacent beads at equilibrium. Structural and dynamical correlations between beads in the Rouse model are thus essentially determined by ζ and K only. The dynamics of such an N -bead Rouse chain under equilibrium conditions (no flow applied) is described by the following Langevin equation:^{21,9}

$$\zeta \frac{\partial \mathbf{R}_n}{\partial t} = - \frac{\partial U}{\partial \mathbf{R}_n} + \mathbf{f}_n \quad \text{for } n = 1, 2, \dots, N \quad (1)$$

where U accounts for the potential energy of the $N-1$ harmonic springs along the chain:

$$U = \sum_{n=1}^{N-1} \frac{1}{2} K (\mathbf{R}_{n+1} - \mathbf{R}_n)^2 \quad (2)$$

In eqs 1 and 2, \mathbf{R}_n denotes the position vector of the n th bead and \mathbf{f}_n the random Brownian force on this bead. According to the fluctuation–dissipation theorem, the force \mathbf{f}_n obeys the following equations:

$$\langle \mathbf{f}_n(t) \rangle = \mathbf{0} \quad (3a)$$

$$\langle f_{n\alpha}(t) f_{m\beta}(t') \rangle = 2\zeta k_B T \delta_{nm} \delta_{\alpha\beta} \delta(t - t') \quad (3b)$$

for $\alpha, \beta = x, y, z$

where δ_{nm} is the Kronecker delta and $\delta(t - t')$ denotes the Dirac delta function. Combining eqs 1 and 2, in the continuum limit (i.e., $N \rightarrow \infty$), we obtain:

$$\zeta \frac{\partial \mathbf{R}_n}{\partial t} = \frac{3k_B T}{b^2} \frac{\partial^2 \mathbf{R}_n}{\partial n^2} + \mathbf{f}_n \quad \text{for } n = 1, 2, \dots, N \quad (4)$$

Equations 1–4 are valid both for linear and ring polymers; where the two systems are distinguished is in the boundary conditions. An N -bead ring polymer possesses structural periodicity since it returns back to itself every N steps; thus the boundary conditions that should complement eq 4 for the case of a ring chain are as follows:

$$\mathbf{R}_0 = \mathbf{R}_N \quad (5a)$$

$$\frac{\partial \mathbf{R}_n}{\partial n} \Big|_{n=0} = \frac{\partial \mathbf{R}_n}{\partial n} \Big|_{n=N} \quad (5b)$$

Here a new hypothetical bead \mathbf{R}_0 whose position coincides with \mathbf{R}_N has been artificially introduced. For the case of a linear chain, the corresponding boundary conditions read: $\partial \mathbf{R}_n / \partial n \Big|_{n=0} = (\partial \mathbf{R}_n / \partial n) \Big|_{n=N} = 0$. Following the corresponding treatment of the Rouse model for linear polymers,⁹ to solve eqs 4 and 5, we introduce the normal coordinates \mathbf{X}_p and \mathbf{Y}_p through

$$\mathbf{R}_n(t) = \mathbf{X}_0 + \sum_{p=1}^{\infty} \left[2\mathbf{X}_p \cos\left(\frac{p\pi n}{N}\right) + 2\mathbf{Y}_p \sin\left(\frac{p\pi n}{N}\right) \right] \quad (6)$$

From the orthogonality relationship between the sine and cosine functions, the expansion coefficients in eq 6 are calculated as

$$\mathbf{X}_p(t) = \frac{1}{N} \int_0^N \mathbf{R}_n(t) \cos\left(\frac{p\pi n}{N}\right) dn \quad \text{for} \\ p = 0, 1, 2, 3, 4, \dots \quad (7a)$$

$$\mathbf{Y}_p(t) = \frac{1}{N} \int_0^N \mathbf{R}_n(t) \sin\left(\frac{p\pi n}{N}\right) dn \quad \text{for} \\ p = 1, 2, 3, 4, \dots \quad (7b)$$

By applying the boundary conditions (eq 5) to eq 6, we find then that all the odd modes should vanish. This implies that

$$\mathbf{R}_n(t) = \mathbf{X}_0 + \sum_{p:\text{even}}^{\infty} \left[2\mathbf{X}_p \cos\left(\frac{p\pi n}{N}\right) + 2\mathbf{Y}_p \sin\left(\frac{p\pi n}{N}\right) \right] \quad (8a)$$

$$\mathbf{X}_p(t) = \frac{1}{N} \int_0^N \mathbf{R}_n(t) \cos\left(\frac{p\pi n}{N}\right) dn \quad \text{for } p = 0, 2, 4, 6, \dots \quad (8b)$$

$$\mathbf{Y}_p(t) = \frac{1}{N} \int_0^N \mathbf{R}_n(t) \sin\left(\frac{p\pi n}{N}\right) dn \quad \text{for } p = 2, 4, 6, 8, \dots \quad (8c)$$

where $p:\text{even}$ in the summation represents only the even modes (i.e., $p = 2, 4, 6, \dots$). Expressions similar to eqs 8 have been reported by Watanabe et al.²³ This particular feature of a ring polymer can be understood by considering that a wave vector that starts from any point (or bead) along the ring should practically complete a full cycle (a wavelength multiplied by an integer value) when it is halfway through its journey, since the way back to the starting point through the other half of the ring is practically the same (the two paths are statistically equivalent). As we will see below, this rather simple but distinctive feature between ring and linear chains results in totally different

predictions of their structural and dynamical properties. For example, by working with the discrete Rouse model in the Appendix, we will see that although the intrinsic time scales of an even mode between a ring and a linear polymer of the same chain length are the same, the corresponding eigenvector(s) are different implying a completely different dynamics or collective motion of beads in the two cases.

In terms of the normal coordinates, the set of the Langevin equations (eq 4) is equivalently written as

$$2N\xi \frac{d\mathbf{X}_p}{dt} = -k_p \mathbf{X}_p + \mathbf{f}_p^X \quad \text{where}$$

$$\mathbf{f}_p^X = 2 \int_0^N \mathbf{f}_n(t) \cos\left(\frac{p\pi n}{N}\right) dn \quad \text{for } p = 0, 2, 4, 6, \dots \quad (9a)$$

$$2N\xi \frac{d\mathbf{Y}_p}{dt} = -k_p \mathbf{Y}_p + \mathbf{f}_p^Y \quad \text{where}$$

$$\mathbf{f}_p^Y = 2 \int_0^N f_n(t) \sin\left(\frac{p\pi n}{N}\right) dn \quad \text{for } p = 2, 4, 6, 8, \dots \quad (9b)$$

where now

$$k_p = \frac{6\pi^2 k_B T}{Nb^2} p^2 \quad \text{for } p = 0, 2, 4, 6, \dots \quad (10)$$

Using eq 3, we also find that:

$$\langle \mathbf{f}_p^X(t) \mathbf{f}_{q\beta}^X(t') \rangle = \langle \mathbf{f}_{p\alpha}^Y(t) \mathbf{f}_{q\beta}^Y(t') \rangle = 0 \quad (11a)$$

$$\langle f_{p\alpha}^X(t) f_{q\beta}^X(t') \rangle = \langle f_{p\alpha}^Y(t) f_{q\beta}^Y(t') \rangle = 4N\xi k_B T \delta_{pq} \delta_{\alpha\beta} \delta(t-t') \quad \text{for } p \neq 0 \text{ or } q \neq 0 \quad (11b)$$

$$\langle f_{0\alpha}^X(t) f_{0\beta}^X(t') \rangle = 8N\xi k_B T \delta_{\alpha\beta} \delta(t-t') \quad (11c)$$

$$\langle f_{p\alpha}^X(t) f_{q\beta}^Y(t') \rangle = 0 \quad \text{for all } p \text{ and } q \quad (11d)$$

eqs 9 for \mathbf{X}_p and \mathbf{Y}_p are decoupled; thus they can be solved independently. The result is:

$$\mathbf{X}_p(t) = \int_{-\infty}^t \frac{1}{2N\xi} \mathbf{f}_p^X(t') \exp[-(t-t')/\tau_p] dt' \quad \text{for } p = 0, 2, 4, 6, \dots \quad (12a)$$

$$\mathbf{Y}_p(t) = \int_{-\infty}^t \frac{1}{2N\xi} \mathbf{f}_p^Y(t') \exp[-(t-t')/\tau_p] dt' \quad \text{for } p = 2, 4, 6, 8, \dots \quad (12b)$$

where

$$\tau_p = \frac{2N\xi}{k_p} = \frac{\xi N^2 b^2}{3\pi^2 k_B T} \frac{1}{p^2} \quad \text{for } p = 2, 4, 6, 8, \dots \quad (13)$$

By making use of eq 11, we also obtain

$$\langle X_{p\alpha}(t) X_{q\beta}(0) \rangle = \delta_{pq} \delta_{\alpha\beta} \frac{k_B T}{k_p} \exp(-t/\tau_p) \quad \text{for } p, q = 0, 2, 4, 6, \dots \quad (14a)$$

$$\langle Y_{p\alpha}(t) Y_{q\beta}(0) \rangle = \delta_{pq} \delta_{\alpha\beta} \frac{k_B T}{k_p} \exp(-t/\tau_p) \quad \text{for } p, q = 2, 4, 6, \dots \quad (14b)$$

Relaxation Time. Equation 13 shows that the characteristic relaxation spectrum of a ring chain bears exactly the same form as that of its linear analogue,⁹ but we should always remember that while all modes are permitted in the latter ($p = 1, 2, 3, 4, \dots$), only even modes are allowed in the former (i.e., $p = 2, 4, 6, 8, \dots$). The longest relaxation (Rouse) time for a ring chain is therefore

$$\tau_{R,ring} = \tau_2 = \frac{\xi N^2 b^2}{12\pi^2 k_B T} \quad (15)$$

This is equal to one-fourth of the corresponding Rouse time for a linear chain comprising the same number of beads N ($\tau_{R,linear} = \tau_1 = \xi N^2 b^2 / 3\pi^2 k_B T$; i.e., $\tau_{R,ring} = \tau_{R,linear}/4$). It is further noted that $\tau_{R,ring}$ corresponds also to the rotational relaxation time describing chain rotation of a ring polymer. Defining the ring diameter vector as $\mathbf{R}_d(t) \equiv \mathbf{R}_{n+N/2}(t) - \mathbf{R}_n(t)$ for $n = 1, 2, \dots, N$, we see from eq 8a that

$$\mathbf{R}_d(t) = -4 \sum_{p=2, 6, 10, 14, \dots}^{\infty} \left[\mathbf{X}_p \cos\left(\frac{p\pi n}{N}\right) + \mathbf{Y}_p \sin\left(\frac{p\pi n}{N}\right) \right] \quad (16)$$

By using the relationships in eq 14, we derive then the following expression for the orientational relaxation of $\mathbf{R}_d(t)$:

$$\begin{aligned} \langle \mathbf{R}_d(t) \cdot \mathbf{R}_d(0) \rangle &= 16 \sum_{p=2, 6, 10, 14, \dots}^{\infty} \left\langle \left(\mathbf{X}_p(t) \cos\left(\frac{p\pi n}{N}\right) \right. \right. \\ &\quad \left. \left. + \mathbf{Y}_p(t) \sin\left(\frac{p\pi n}{N}\right) \right) \cdot \left(\mathbf{X}_p(0) \cos\left(\frac{p\pi n}{N}\right) \right. \right. \\ &\quad \left. \left. + \mathbf{Y}_p(0) \sin\left(\frac{p\pi n}{N}\right) \right) \right\rangle \\ &= 48 \sum_{p=2, 6, 10, 14, \dots}^{\infty} \frac{k_B T}{k_p} \exp(-t/\tau_p) \\ &= Nb^2 \sum_{p=2, 6, 10, 14, \dots}^{\infty} \frac{8}{\pi^2} \frac{1}{p^2} \exp(-t/\tau_p) \end{aligned} \quad (17)$$

This result resembles the corresponding expression for the time autocorrelation function of the chain end-to-end vector \mathbf{R} for a linear chain (for which, of course, $p = 1, 3, 5, \dots$ in the summation instead of $p = 2, 6, 10, \dots$). From eq 17, it is readily found that $\langle R_d^2 \rangle = Nb^2/4$; this is equal to one-fourth of the mean square chain end-to-end distance $\langle R^2 \rangle = Nb^2$ of the linear analogue. We further note that $\langle R_d^2 \rangle$ is only the half of $\langle R^2 \rangle = Nb^2/2$ of the corresponding linear polymer with $N/2$ beads, indicating a more compact structure of ring chains compared to linear ones due to their looped topology. Equation 17 can also be rewritten as

$$\langle \mathbf{R}_d(t) \cdot \mathbf{R}_d(0) \rangle / \langle R_d^2 \rangle = \sum_{p=2, 6, 10, 14, \dots}^{\infty} \frac{32}{\pi^2} \frac{1}{p^2} \exp(-t/\tau_p) \quad (18)$$

In a similar way, we can derive an expression for the mean square radius of gyration $\langle R_g^2 \rangle$ of a ring polymer. To this, we

note from eq 8b that \mathbf{X}_0 coincides with the center-of-mass position

$$\mathbf{R}_G = \frac{1}{N} \int_0^N \mathbf{R}_n \, dn$$

of the chain. With the help of eq 14 then, the following expression is obtained for $\langle R_g^2 \rangle$ for a ring chain:

$$\begin{aligned} \langle R_g^2 \rangle &= \frac{1}{N} \sum_{n=1}^N \langle (\mathbf{R}_n - \mathbf{R}_G)^2 \rangle \\ &= \frac{1}{N} \sum_{n=1}^N \left\langle \left(\sum_{p;even}^{\infty} \left[2\mathbf{X}_p \cos\left(\frac{p\pi n}{N}\right) + 2\mathbf{Y}_p \sin\left(\frac{p\pi n}{N}\right) \right] \right)^2 \right\rangle \\ &= \frac{4}{N} \sum_{p;even}^{\infty} \left[\langle \mathbf{X}_p^2 \rangle \int_0^N \cos^2\left(\frac{p\pi n}{N}\right) \, dn \right. \\ &\quad \left. + \langle \mathbf{Y}_p^2 \rangle \int_0^N \sin^2\left(\frac{p\pi n}{N}\right) \, dn \right] \\ &= 2 \sum_{p;even}^{\infty} (\langle \mathbf{X}_p^2 \rangle + \langle \mathbf{Y}_p^2 \rangle) = \frac{1}{12} N b^2 \end{aligned} \quad (19)$$

The value of $\langle R_g^2 \rangle$ for a ring polymer is thus equal to one-half that of the corresponding linear analogue. Exactly the same result has been obtained by Kramers¹⁶ and Zimm and Stockmayer.¹⁷

Diffusion Coefficient. According to eq 9a, the dynamics of $\mathbf{X}_0 (= \mathbf{R}_G)$ is governed by the following equation:

$$\frac{d\mathbf{X}_0}{dt} = \frac{1}{2N\xi} \mathbf{f}_0^X \quad (20)$$

which can be integrated to give:

$$\mathbf{X}_0(t) = \mathbf{X}_0(0) + \int_0^t \frac{1}{2N\xi} \mathbf{f}_0^X(t') \, dt' \quad (21)$$

Using eq 11c, we find then that

$$\begin{aligned} &\langle (X_{0\alpha}(t) - X_{0\alpha}(0))(X_{0\beta}(t) - X_{0\beta}(0)) \rangle \\ &= \left(\frac{1}{2N\xi} \right)^2 \int_0^t \int_0^t \langle f_{0\alpha}(t') f_{0\beta}(t'') \rangle \, dt' \, dt'' = \frac{2k_B T}{N\xi} \delta_{\alpha\beta} t \end{aligned} \quad (22)$$

which implies that

$$\langle (\mathbf{R}_G(t) - \mathbf{R}_G(0))^2 \rangle = \frac{6k_B T}{N\xi} t \quad (23)$$

By the Einstein argument then, the center-of-mass diffusion coefficient D_G is found to be given by:

$$D_G = \lim_{t \rightarrow \infty} \frac{\langle (\mathbf{R}_G(t) - \mathbf{R}_G(0))^2 \rangle}{6t} = \frac{k_B T}{N\xi} \quad (24)$$

which is identical to the corresponding expression of the Rouse model for the linear polymer of the same chain length N .⁹ Such a result should have been expected since in the Rouse model no hydrodynamic interactions are considered, thus a bead moves *independently* of the others subject only to the frictional force governed by the drag coefficient ξ . But such a behavior is independent of the molecular architecture of the chain, thus eq 24 should be valid for any type of chains composed of N beads that obey Rouse dynamics.

Viscoelasticity. In the continuous limit ($N \rightarrow \infty$), the stress tensor is expressed as^{2,9}

$$\begin{aligned} \sigma_{\alpha\beta} &= \frac{1}{V} \left\langle \sum_{i=1}^l \sum_{n=1}^N R_{in,\alpha} F_{in,\beta} \right\rangle \\ &= \frac{lK}{V} \int_0^N \left\langle \frac{\partial R_{n\alpha}}{\partial n} \frac{\partial R_{n\beta}}{\partial n} \right\rangle \, dn \\ &= \frac{l}{V} \sum_{p;even}^{\infty} k_p (\langle X_{p\alpha}(t) X_{p\beta}(t) \rangle + \langle Y_{p\alpha}(t) Y_{p\beta}(t) \rangle) \end{aligned} \quad (25)$$

where l denotes the number of molecules in the system and V the volume. To compute $\langle X_{p\alpha}(t) X_{p\beta}(t) \rangle$ and $\langle Y_{p\alpha}(t) Y_{p\beta}(t) \rangle$, we note first that in the presence of an externally applied flow field represented by the velocity gradient tensor ∇v , the right-hand side of eq 1 should contain an additional term equal to $\mathbf{R}_n \cdot \nabla v$. Expressing the resulting equation in terms of the normal coordinates and taking the ensemble average leads then to the following two time dependent equations for $\langle X_{p\alpha}(t) X_{p\beta}(t) \rangle$ and $\langle Y_{p\alpha}(t) Y_{p\beta}(t) \rangle$:

$$\begin{aligned} \frac{\partial \langle X_{p\alpha} X_{p\beta} \rangle}{\partial t} &= \frac{1}{2N\xi} (2k_B T \delta_{\alpha\beta} - 2k_p \langle X_{p\alpha} X_{p\beta} \rangle) \\ &\quad + \nabla_\mu v_\alpha \langle X_{p\mu} X_{p\beta} \rangle + \nabla_\mu v_\beta \langle X_{p\mu} X_{p\alpha} \rangle \end{aligned} \quad (26a)$$

$$\begin{aligned} \frac{\partial \langle Y_{p\alpha} Y_{p\beta} \rangle}{\partial t} &= \frac{1}{2N\xi} (2k_B T \delta_{\alpha\beta} - 2k_p \langle Y_{p\alpha} Y_{p\beta} \rangle) \\ &\quad + \nabla_\mu v_\alpha \langle Y_{p\mu} Y_{p\beta} \rangle + \nabla_\mu v_\beta \langle Y_{p\mu} Y_{p\alpha} \rangle \end{aligned} \quad (26b)$$

where the Einstein summation convention has been tacitly assumed for repeated indices: if a certain index occurs twice in a term in the expression, the term is assumed to be summed over the repeated index for all admissible values of the index, e.g.

$$a_\alpha b_\alpha = \sum_{\alpha=1}^3 a_\alpha b_\alpha$$

in three-dimensional coordinate systems. The two expressions in eq 26 have exactly the same mathematical structure, thus $\langle X_{p\alpha} X_{p\beta} \rangle = \langle Y_{p\alpha} Y_{p\beta} \rangle$. To solve eq 26 we need to know the type of flow applied on the system. Let us consider here the case of simple shear. For this type of flow, only the term $\nabla_y v_x (\equiv \dot{\gamma})$ is nonzero; from eq 26a we find then that:

$$\frac{\partial \langle X_{py}^2 \rangle}{\partial t} = - \frac{k_p}{N\xi} \langle X_{py}^2 \rangle + \frac{k_B T}{N\xi} \quad (27a)$$

$$\frac{\partial \langle X_{px} X_{py} \rangle}{\partial t} = - \frac{k_p}{N\xi} \langle X_{px} X_{py} \rangle + \dot{\gamma} \langle X_{py}^2 \rangle \quad (27b)$$

To solve eq 27, we distinguish between two cases: (i) steady-state shear and (ii) small amplitude oscillatory shear.

(i). *Simple Shear under Steady-State Conditions:* $\dot{\gamma} = \dot{\gamma}_0$. Under steady-state conditions, eq 27 leads to:

$$\langle X_{py}^2 \rangle = \frac{k_B T}{k_p} \quad (28a)$$

$$\langle X_{px} X_{py} \rangle = \frac{N\xi}{k_p} \dot{\gamma}_0 \langle X_{py}^2 \rangle = \frac{N\xi k_B T}{k_p^2} \dot{\gamma}_0 \quad (28b)$$

Substitution into eq 25 gives:

$$\sigma_{xy}(t) = \frac{l}{V} \sum_{p;even}^{\infty} \frac{2N\zeta k_B T}{k_p} \dot{\gamma}_0 \quad (29)$$

from which we can easily calculate the viscosity

$$\begin{aligned} \eta_{ring} &\equiv \frac{\sigma_{xy}(t)}{\dot{\gamma}_0} = \frac{l}{V} \sum_{p;even}^{\infty} \frac{2N\zeta k_B T}{k_p} = \frac{lk_B T}{V} \sum_{p;even}^{\infty} \frac{1}{\tau_p} \\ &= \frac{\pi^2 lk_B T \tau_{R,ring}}{6 V} \end{aligned} \quad (30)$$

Comparing eq 30 with the corresponding result of the Rouse model for a melt of linear chains of the same chain length N , namely $\eta_{linear} = (\pi^2/12)lk_B T \tau_{R,linear}/V$, and using that $\tau_{R,ring} = \tau_{R,linear}/4r$, we conclude that $\eta_{ring} = \eta_{linear}/2$, a result fully consistent with the findings of ref 19.

(ii). Small Amplitude Oscillatory Shear: $\dot{\gamma} = \dot{\gamma}_0 \text{Re}[\exp(i\omega t)]$. In this case and for small $\dot{\gamma}_0$, we may put $\langle X_{py}^2 \rangle \approx k_B T/k_p$. From eq 27b and defining $\tau'_p = N\zeta/k_p$ ($= \tau_p/2$), then we get

$$\langle X_{px} X_{py} \rangle = \frac{k_B T}{k_p} \int_{-\infty}^t \exp[-(t-t')/\tau'_p] \dot{\gamma}(t') dt' \quad (31)$$

which can be substituted back into eq 25 to give

$$\sigma_{xy}(t) = \frac{2lk_B T}{V} \sum_{p;even}^{\infty} \int_{-\infty}^t \exp[-(t-t')/\tau'_p] \dot{\gamma}(t') dt' \quad (32)$$

Comparing this equation with the corresponding expression for the general linear viscoelastic model,² namely

$$\sigma_{xy}(t) = \int_{-\infty}^t G(t-t') \dot{\gamma}(t') dt'$$

we come up with the following expression for the relaxation modulus $G(t)$:

$$\begin{aligned} G(t) &= \frac{2lk_B T}{V} \sum_{p;even}^{\infty} \exp(-t/\tau'_p) \\ &= \frac{2\rho RT}{M} \sum_{p;even}^{\infty} \exp(-t/\tau'_p) \end{aligned} \quad (33)$$

from which, next, one can easily compute the storage $G'(\omega)$ and loss $G''(\omega)$ moduli of the melt:

$$\begin{aligned} G'(\omega) &= \int_0^{\infty} \omega \sin(\omega t) G(t) dt \\ &= \frac{2\rho RT}{M} \sum_{p;even}^{\infty} \frac{(\omega \tau'_p)^2}{1 + (\omega \tau'_p)^2} \end{aligned} \quad (34a)$$

$$\begin{aligned} G''(\omega) &= \int_0^{\infty} \omega \cos(\omega t) G(t) dt \\ &= \frac{2\rho RT}{M} \sum_{p;even}^{\infty} \frac{\omega \tau'_p}{1 + (\omega \tau'_p)^2} \end{aligned} \quad (34b)$$

The corresponding expressions of the model for linear chains can be found (e.g.) on p 115 of ref 9. We also note in the

passing that, in accordance with the general linear viscoelastic model

$$\eta_{ring} = \int_0^{\infty} G(t) dt$$

Dynamic Structure Factor. The starting expression for the calculation of the dynamic structure factor $S(\mathbf{q},t)$ is⁹

$$\begin{aligned} S(\mathbf{q},t) &= \frac{1}{N} \sum_{n=1}^N \sum_{m=1}^N \langle \exp[i\mathbf{q} \cdot (\mathbf{R}_n(t) - \mathbf{R}_m(0))] \rangle \\ &= \frac{1}{N} \sum_{n=1}^N \sum_{m=1}^N \exp \left[-\frac{1}{6} q^2 \phi_{nm}(t) \right] \end{aligned} \quad (35)$$

In eq 35, $\phi_{nm}(t) \equiv \langle (\mathbf{R}_n(t) - \mathbf{R}_m(0))^2 \rangle$ where $\mathbf{R}_n(t)$ denotes the position vector of chain segment n along the chain at time t . Also, \mathbf{q} is the scattering vector with a magnitude q equal to

$$q = \frac{4\pi}{\lambda} \sin\left(\frac{\theta}{2}\right)$$

where λ is the wavelength of the radiation and θ the scattering angle.

With the help of eqs 8a, 14, and 22, $\phi_{nm}(t)$ for ring polymers comes out to be

$$\begin{aligned} \phi_{nm}(t) &= 6D_G t + \phi_{nm}(0) \\ &+ \frac{4Nb^2}{\pi^2} \sum_{p;even}^{\infty} \frac{1}{p^2} \cos\left(\frac{p\pi}{N}(n-m)\right) (1 - \exp(-p^2 t / 4\tau_{R,ring})) \end{aligned} \quad (36)$$

where

$$\phi_{nm}(0) = \frac{|n-m|(N-|n-m|)}{N} b^2 \quad (37)$$

an expression first derived by Zimm and Stockmayer.¹⁷ The corresponding expression for linear polymers is:⁹

$$\begin{aligned} \phi_{nm}(t) &= 6D_G t + \phi_{nm}(0) \\ &+ \frac{4Nb^2}{\pi^2} \sum_{p=1}^{\infty} \frac{1}{p^2} \cos\left(\frac{p\pi n}{N}\right) \cos\left(\frac{p\pi m}{N}\right) (1 - \exp(-p^2 t / \tau_{R,linear})) \end{aligned} \quad (38)$$

where now

$$\phi_{nm}(0) = |n-m|b^2 \quad (39)$$

The above expressions show that the behavior of $S(\mathbf{q},t)$ between ring and linear polymers is different at small and intermediate time scales but the same at long time scales (since, in both cases, at long enough times: $\phi_{nm}(t) \sim 6D_G t$).

3. Molecular Model and Systems Studied

A molecular model which has been shown to provide reliable predictions of the thermodynamic, structural, and dynamic properties of linear and nonlinear PE melt systems over a wide range of temperature conditions⁷⁶ has been adopted in the present simulations with the ring PE systems. The model makes use of a united-atom (UA) description for the representation of PE rings, according to which every carbon atom along the chain together with the two hydrogen atoms attached to it is treated as a

single Lennard-Jones interaction site (we call this a methylene unit). Bond-stretching interactions are described then by a harmonic potential function of the form:

$$U_{\text{stretching}}(l) = \frac{k_{\text{str}}}{2}(l - l_0)^2 \quad (40)$$

with values (shown in Table 1) for the parameters k_{str} and l_0 describing the stiffness of the spring and the equilibrium bond-length, respectively, borrowed from the work of Nath and Khare.⁷⁷ A harmonic potential of the form

$$U_{\text{bending}}(\theta) = \frac{k_\theta}{2}(\theta - \theta_0)^2 \quad (41)$$

describes interactions associated with every bond bending skeletal angle θ ; values for the parameters k_θ and θ_0 have been proposed by Van der Ploeg and Berendsen⁷⁸ and are also listed in Table 1. The bond-torsional potential associated with the dihedral angle ϕ is described by the nine-term cosine series proposed by Toxvaerd:⁷⁹

$$U_{\text{torsional}}(\phi)/k_B = \sum_{i=0}^8 c_i \cos^i(\phi) \quad (42)$$

with the values of coefficients c_i reported in Table 1. All nonbonded interactions [intermolecular interactions between atoms belonging to different molecules, and intramolecular interactions between atoms separated by more than three bonds in the

Table 1. Values of the Force-Field Parameters Defining the Bond Stretching (Taken from Ref 77), Bond Bending (Taken from Ref 78), Bond Torsional (Taken from Ref 79), and Nonbonded Lennard-Jones (Taken from Ref 80) Potential Functions

interaction type	interaction sites	model parameters
bond stretching	CH ₂ —CH ₂	$k_{\text{str}} = 96500 \text{ K}/\text{\AA}^2$ $l_0 = 1.54 \text{ \AA}$
bond bending	CH ₂ —CH ₂ —CH ₂	$k_\theta = 62500 \text{ K}/\text{rad}^2$ $\theta_0 = 114^\circ$
bond torsional	CH ₂ —CH ₂ —CH ₂ —CH ₂	$c_0 = 1001 \text{ K}$ $c_1 = 2130 \text{ K}$ $c_2 = -303 \text{ K}$ $c_3 = 3612 \text{ K}$ $c_4 = 2227 \text{ K}$ $c_5 = 1966 \text{ K}$ $c_6 = -4489 \text{ K}$ $c_7 = -1736 \text{ K}$ $c_8 = 2817 \text{ K}$
nonbonded Lennard-Jones	CH ₂	$\sigma = 3.95 \text{ \AA}$ $\epsilon/k_B = 46 \text{ K}$

same molecule] are described by a standard 12–6 Lennard–Jones potential of the form:

$$U_{\text{LJ}}(r) = 4\epsilon \left[\left(\frac{\sigma}{r} \right)^{12} - \left(\frac{\sigma}{r} \right)^6 \right] \quad (43)$$

with the values of the constants ϵ and σ taken from the TraPPE model⁸⁰ as shown in Table 1.

Using the molecular model described by eqs 40–43, 11 different ring PE systems ranging in molecular length from C₂₄ to C₄₀₀ were simulated in this work. Their detailed characteristics are reported in Table 2 where one can see that sufficiently large simulation cells were employed in all cases to avoid finite system size effects. For each system, the initial configuration was created in three steps by making use of the Materials Studio software package,⁸¹ as follows: (i) In the first step, we initially built one chain of a given size (equal to the number of carbon atoms per chain for the system under study), which was then copied as many times as possible in 3-d space to generate a finite model structure; we also chose the dimensions of the simulation box carefully to completely avoid any chain concatenation. (ii) In the second step, this initial configuration was subjected to a potential energy minimization procedure. At the end of this procedure, we inspected again the resulting configuration as thoroughly as possible (practically chain-by-chain) to confirm the complete absence of any ring concatenation. (iii) In the third step, the final configuration from step (ii) was subjected to an exhaustive pre-equilibration run via a long *NPT* MD simulation at $T = 600 \text{ K}$ and $P = 1 \text{ atm}$. A fully equilibrated system configuration thus obtained was used as the initial configuration for the production run (an *NPT* MD simulation) with the given system at the conditions of interest ($T = 450 \text{ K}$ and $P = 1 \text{ atm}$). All atomistic MD simulations were carried out in the isothermal–isobaric (*NPT*) statistical ensemble by making use of the Nosé–Hoover thermostat–barostat^{82–85} to maintain the temperature T and pressure P fixed at their prescribed values of $T = 450 \text{ K}$ and $P = 1 \text{ atm}$.

For the integration of the equations of motion, the very efficient multiple-time-step algorithm *r*-RESPA (reversible reference system propagator algorithm)⁸⁶ was used with two different time scales: a short time scale $dt = 0.5 \text{ fs}$ for the integration of the fast-varying forces (bond-stretching, bond-bending, and bond-torsional interactions), and a long time scale $\Delta t = 4dt$ for the integration of the slowly varying forces (the nonbonded Lennard–Jones interactions and the equations for the Nosé–Hoover thermostat–barostat). The duration of the MD runs varied from 50 ns for the shorter (C₂₄, C₃₂) to 1 μs for the longer (C₃₂₀, C₄₀₀) systems. All MD runs were carried out with the large-scale atomic/molecular massively parallel simulator (LAMMPS)^{87,88}

Table 2. Simulation Results for the Density ρ , the Mean-Square Ring Diameter $\langle R_d^2 \rangle$, the Mean-Square Chain Radius of Gyration $\langle R_g^2 \rangle$, and the Packing Length l_p of the Simulated PE Ring Melts at $P = 1 \text{ atm}$, $T = 450 \text{ K}$, and Comparison with the Corresponding Results for the Linear Analogues

system ^a	$\rho (\text{g}/\text{cm}^3)$	ring PE				linear PE ^c		
		$\langle R_d^2 \rangle (\text{\AA}^2)$	$\langle R_g^2 \rangle (\text{\AA}^2)$	$\langle R_d^2 \rangle/\langle R_g^2 \rangle$	$l_p (\text{\AA})^b$	$\rho (\text{g}/\text{cm}^3)$	$\langle R_g^2 \rangle (\text{\AA}^2)$	$l_p (\text{\AA})^b$
C ₂₄ (192)	0.753	78 ± 10	20 ± 4	3.9	37.0	0.694		
C ₃₂ (108)	0.762	118 ± 10	31.5 ± 5	3.7	31.0	0.700	70 ± 8	16.2
C ₄₈ (81)	0.769	220 ± 10	55.5 ± 5	3.6	26.2	0.742	111 ± 8	13.6
C ₆₀ (81)	0.772	261 ± 15	74 ± 8	3.5	24.4			
C ₇₈ (54)	0.773	345 ± 30	101 ± 10	3.4	23.2	0.749	208 ± 10	11.6
C ₁₀₀ (54)	0.773	437 ± 20	132 ± 10	3.3	22.8	0.754	292 ± 15	10.6
C ₁₂₀ (54)	0.773	516 ± 30	160 ± 10	3.2	22.5	0.757	340 ± 20	11.0
C ₁₇₄ (54)	0.774	710 ± 40	230 ± 18	3.1	22.7	0.762	528 ± 20	10.1
C ₂₂₄ (54)	0.774	870 ± 80	290 ± 20	3.0	23.2	0.765	695 ± 20	9.8
C ₃₂₀ (32)	0.775	1100 ± 80	385 ± 30	2.9	24.9	0.767	980 ± 30	9.9
C ₄₀₀ (54)	0.775	1450 ± 100	470 ± 30	3.1	25.5	0.768	1290 ± 30	9.4

^a Number in parentheses indicates the number of chains employed in the simulation of the rings. ^b Calculated using eq 44. ^c Data from ref 76.

code, that can run on any parallel platform supporting the MPI library.

4. Results and Discussion

4.1. Structural Properties. Chain Conformations. The conformational properties of the simulated ring PE melts have been analyzed in terms of the mean-square chain radius of gyration $\langle R_g^2 \rangle$ and the mean-square ring diameter $\langle R_d^2 \rangle$. Results for $\langle R_d^2 \rangle$ and $\langle R_g^2 \rangle$ for all the simulated PE ring melts are presented in Table 2. They show that the ratio $\langle R_d^2 \rangle/\langle R_g^2 \rangle$, which is somewhat larger than 3 for the shortest rings, becomes smaller and smaller as the chain length increases, approaching eventually a value equal to 3 for rings with $N > 120$, exactly as predicted by the Rouse theory (see eqs 17 and 19 of section 2 above). Also reported in Table 2 are $\langle R_g^2 \rangle$ results for the corresponding linear PE melts from atomistic simulations with the same molecular model.⁷⁶ A direct comparison of the $\langle R_g^2 \rangle$ data between ring and linear PE melts reveals that, for the same chain length N , the average dimension of a ring polymer is always smaller than that of its linear analogue. This is due to the more symmetric arrangement of carbon atoms around the chain center-of-mass in rings, which, in turn, leads to a more compact overall structure in their melt state. It is also consistent with the findings of other simulation^{27–30,64,65,67–70} and experimental studies of rings in melts and solutions.^{24,89,51,52,54} More precisely, our simulation data show that for $N < 174$ the ratio $\langle R_g^2 \rangle_{\text{linear}}/\langle R_g^2 \rangle_{\text{ring}}$ of the radius of gyration of a linear PE chain over the radius of gyration of the corresponding ring PE chain is approximately equal to 2.1 ± 0.1 , a result which verifies the theoretical analysis of Kramers¹⁶ and Zimm and Stockmayer¹⁷ (see also eq 19). For $N > 174$, on the other hand, the ratio is found to increase with increasing N (see, e.g., Figure 1a). As shown in the inset of Figure 1a, the value of the exponent ν in the scaling $R_g \sim N^\nu$ decreases as N increases, approaching a value equal to $\nu = 0.43 \pm 0.02$ for $N > 174$ as opposed to the value $\nu = 0.5$ for the corresponding linear chains. In addition, the “ideal” scaling $R_g \sim N^{0.5}$ for ring PE melts seems to be sandwiched in a rather narrow region of chain lengths; according to the simulation results (Figure 1a), this region lies approximately between $60 < N < 120$. Such an apparent ideal scaling is considered to have arisen from the canceling effect of the non-Gaussian chain structure (leading to an increase of the power exponent) and the nonconcatenation topological constraint (leading to a decrease of the power exponent). Similar results have also been reported in the literature either through computer simulations^{28,34,47,48,67,68,71,55} or through experimental measurements.^{24,25,89,90} For example, Hur et al.²⁷ found that $\nu = 0.45$ for $N > 100$ from atomistic MD simulations of ring PE melts, while the simulation studies of Muller et al.,^{29,30} Brown and Szamel,^{28,31,67} and Deutsch and Cates^{34,68} with the bond fluctuation model indicated ν values equal to 0.45, 0.42, and 0.4, respectively. A somewhat smaller value ($\nu = 0.42 \pm 0.05$) has been reported by Arrighi et al.²⁴ based on neutron scattering experiments with polydimethylsiloxane (PDMS) rings.

In general, the value of the exponent ν for ring polymer melts is believed to decrease with increasing N , approaching eventually the value $1/3$ for truly long rings (high enough N) corresponding to collapsed structures.³⁰ We mention, for example, the recent simulation studies of Vettorel et al.^{64,65} with an on-lattice Monte Carlo model and of Suzuki et al.^{26,72} with the BFM which showed a gradual decrease of ν with N toward the asymptotic value of $1/3$ at high enough N 's. From a physical point of view, the shrinkage of a ring chain as its chain length N increases is associated with the architectural restrictions imposed by ring nonconcatenation, which gives rise to an effective pressure that tends to squeeze ring chains against each other. It is a picture fully

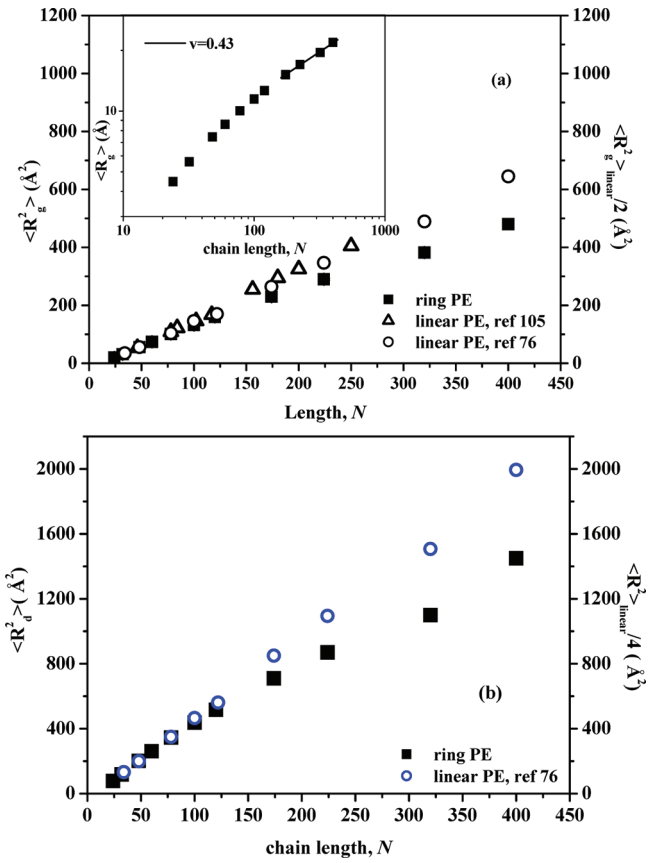


Figure 1. Dependence of ring size on chain length and comparison with the scaling laws of the Rouse theory ($T = 450$ K and $P = 1$ atm): (a) the average square of the ring radius of gyration $\langle R_g^2 \rangle$ (left axis) versus the one-half of the corresponding value for the linear analogue $\langle R_g^2 \rangle_{\text{linear}}/2$ (right axis), and (b) the average square of the ring diameter $\langle R_d^2 \rangle$ (left axis) versus the one-fourth of the square end-to-end distance of the corresponding linear analogue $\langle R^2 \rangle_{\text{linear}}/4$ (right axis). The data for the linear systems have been taken from refs 105 and 76. The error bars in all cases are commensurate with the size of the symbols used to represent the data.

supported by the simulation findings of Brown et al.,^{28,31} where nonconcatenation was observed to cause a significant reduction in the size of rings in melt (in sharp contrast to the case of isolated rings where the corresponding effect is for all practical purposes negligible).

Figure 1b presents the dependence of $\langle R_d^2 \rangle$ on chain length for the simulated ring melts; the results are shown together with simulation data for the mean-square chain end-to-end distance $\langle R^2 \rangle$ of linear analogues. We remind the reader that, if the simulated ring chains behaved identically as Rouse chains, then $\langle R_d^2 \rangle$ should be equal to $\langle R^2 \rangle/4$ (see eq 17 above). The simulation data are consistent with such a relationship only for chains with $N < 174$. For longer rings, significant differences are observed between the two sets of data, indicating strong deviations of the simulation results from the Rouse scaling.

An important measure of the structure of a polymeric chain is the packing length l_p , since it is related with the rheological and topological properties of system (for example, it determines the entanglement molecular weight of the polymer). For branched or ring chain architectures, l_p is defined as⁹¹

$$l_p = \frac{M}{\rho N_A \langle R_g^2 \rangle} \quad (44)$$

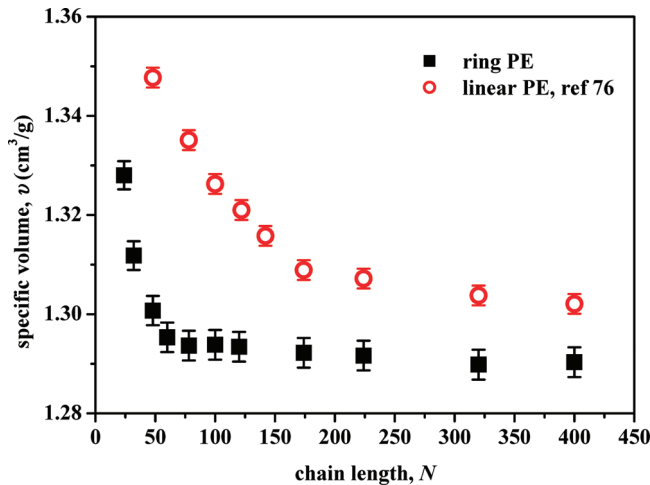


Figure 2. Chain length dependence of the specific volume v of the simulated ring PE (close symbols) and linear PE systems (open symbols) obtained from ref 76.

where ρ is the system density, M the chain molecular weight, and N_A Avogadro's number. For a given melt density and chain length N or molecular weight M , therefore, l_p will attain larger values for chains characterized by smaller $\langle R_g^2 \rangle$ values, i.e., for chains that assume more compact structures. Our simulation data for the packing length of all systems studied here are reported in Table 2 and demonstrate that ring chains are characterized by l_p values that are significantly larger (by a factor of 2–3) than those of the corresponding linear analogues. In turn, this is an indication that topological interactions between chains in melts of linear chains are stronger than in melts of ring chains of the same chain length N , a conclusion which is supported by experimental measurements^{39,40,42} of the plateau modulus which in general is found to be smaller in melts of ring chains than in melts of linear ones.

Thermodynamic Properties. Figure 2 presents the variation of the specific volume v of the simulated ring PE systems with the chain length N ; the specific volume of linear PE systems is also shown in the figure for comparison. Ring melts are seen to reach the characteristic asymptotic polymeric regime (where no variation of the system density with molecular weight is observed) at significantly lower N values than linear ones: more precisely, for the PE systems analyzed here, the plateau value of the density, equal to $0.773 \pm 0.002 \text{ g/cm}^3$ for ring chains, is attained for $N > 50$ whereas for the corresponding linear chains the plateau is attained for $N > 200$. It is also interesting that due to absence of chain ends in rings, the density of the ring melts is always higher than that of the corresponding linear systems of the same molecular weight. Of course, the difference in the density of the two types of melts depends on their chain length and decreases with increasing chain length, becoming (for example) less than 1% for $N = 320$. A similar behavior has been reported in previous simulation²⁷ and experimental studies.⁴⁸

In Figure 3a, we present results for the thermal expansion coefficient α_P defined as

$$\alpha_P = \frac{1}{v} \left(\frac{\partial v}{\partial T} \right)_P \quad (45)$$

of the simulated C_{78} ring PE system in a wide range of temperatures, from 300 to 600 K. Our results show that both the specific volume v (see inset in Figure 3a) and the thermal

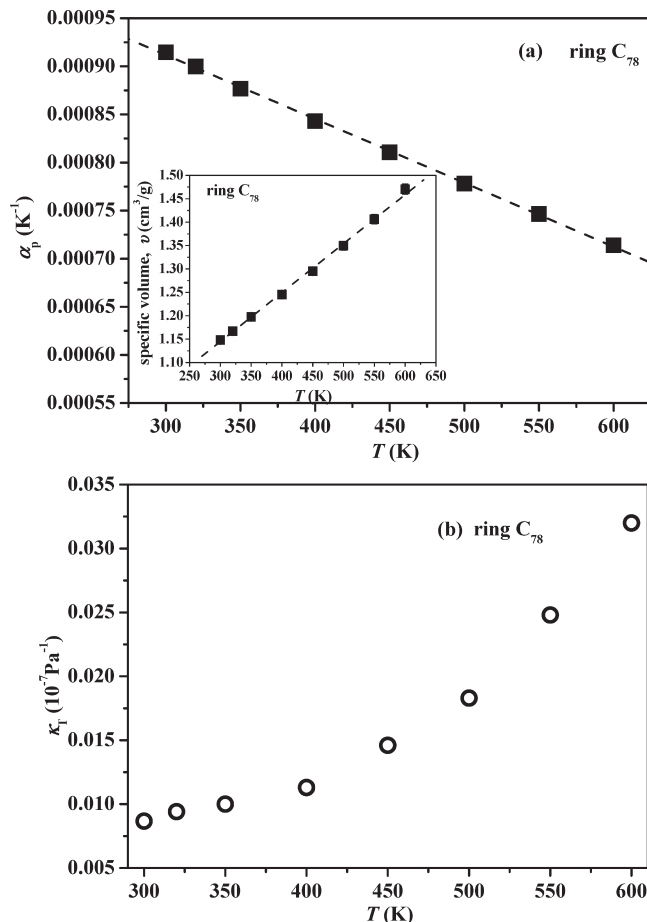


Figure 3. Temperature dependence of (a) the thermal expansion coefficient α_P calculated through eq 45 and (b) the isothermal compressibility κ_T calculated through eq 46b for the C_{78} ring PE system. The inset in part a shows the temperature dependence of the specific volume v of the system. Dashed lines represent the best linear fits to simulation data.

expansion coefficient α_P change linearly with the temperature T at least in the temperature range investigated in the present simulations. For α_P , a similar trend has been recorded in MD simulations with other polymers such as linear *cis*-1,4-polybutadiene and linear polyisobutylene.^{92,93} Furthermore, the values of α_P found from the simulations with the C_{78} ring PE are very similar to those reported in the literature for linear PE. For example, Olabisi and Simha⁹⁴ report a value of α_P equal to $7.81 \times 10^{-4} \text{ K}^{-1}$ in the temperature range 293–388 K and $P = 1 \text{ atm}$ based on fittings of measured experimental density data with the Tait equation, while the atomistic simulations of Gestoso and Karayannidis⁹⁵ with a linear C_{78} PE system point to a value of α_P equal to $7.48 \times 10^{-4} \text{ K}^{-1}$ in the temperature range 250–600 K. And the same holds for the data reported for PE by Wilson and Simha^{96,97} according to which the value of α_P changes from 7.99×10^{-4} to $7.82 \times 10^{-4} \text{ K}^{-1}$ in the temperature range 423–473 K.

Another important thermodynamic parameter that can be calculated easily from the atomistic simulations is the isothermal compressibility defined as

$$\kappa_T = - \frac{1}{v} \left(\frac{\partial v}{\partial P} \right)_T \quad (46a)$$

Alternatively, κ_T can be computed by monitoring volume fluctuations in atomistic simulations in the *NPT*

Table 3. MD Simulation Predictions for the Isothermal Compressibility κ_T of the Ring PE Melts Addressed Here at $P = 1$ atm, $T = 450$ K (Obtained with the Help of eq 46b)

system	$\kappa_T (\times 10^{-9} \text{ Pa}^{-1})$
C_{24}	1.68
C_{32}	1.64
C_{48}	1.32
C_{60}	1.48
C_{78}	1.46
C_{100}	1.46
C_{120}	1.45
C_{174}	1.44
C_{320}	1.41
C_{400}	1.40

statistical ensemble:

$$\kappa_T = \frac{\langle V^2 \rangle - \langle V \rangle^2}{k_B T \langle V \rangle} \quad (46b)$$

Equation 46b is, in fact, a more convenient expression to use than eq 46a, since it allows computing κ_T by carrying out a single *NPT* simulation (and not a number of different simulations at several P values). Simulation results for κ_T for the C_{78} ring PE melt are reported in Figure 3b showing that κ_T increases rapidly with increasing temperature (exactly as observed for linear PE). However, a simple comparison between ring and linear PE (based on the simulation findings for the C_{78} system) reveals that κ_T for the ring PE system is about 10–15% lower than for the corresponding linear system;⁹⁸ ring PE melts are therefore less compressible than linear ones. Clearly, this should be attributed to the more compact and denser structure of the ring systems due to their looped structure and the complete absence of chain ends. Another interesting result of our simulations is that the value of κ_T varies with the molecular weight of the simulated PE rings (see data listed in Table 3). For example, we see that κ_T decreases by approximately 15% as the chain length increases from C_{24} to C_{400} ; this is seen to be closely related to the corresponding variation of the specific volume of the simulated ring systems with the chain length, as reported in Figure 2.

Pair Correlation Function. Significant insight into the structural properties of the simulated PE rings is obtained by the calculation of the intermolecular pair distribution function, $g(r)$. Typical $g(r)$ -vs- r curves for three of the simulated ring PE systems (C_{48} , C_{100} , and C_{224}) at $T = 450$ K are presented in Figure 4a. Similar to the corresponding curves from simulations with the linear analogues,⁹⁹ the curves in all cases exhibit two characteristic peaks: one at around 5.2 Å representing the relative distance for the first intermolecular neighbors and another (less pronounced) at 10.7 Å associated with the second shell of intermolecular neighbors. The position of the first-peak seems to shift slightly to smaller distances as the chain length increases; this reflects the more condensed structure characterizing higher molecular weight ring PE melts. The correlation hole effect, which is more pronounced for the rings with the higher chain length, is also evident in the figure.

How the intermolecular pair distribution functions compare between rings and linear PE melts of the same chain length (C_{120} and C_{320}) is analyzed in Figure 4b. Our results show clearly that the $g(r)$ curves for the ring melts are below those for the linear ones, indicating a stronger correlation hole effect in the former and thus a rather strong effect of molecular architecture on local melt structure. Similar results have been reported by Brown and Szamel.^{28,67} The same conclusion is drawn if we look at the pair correlation function at the level of the chain center-of-mass,

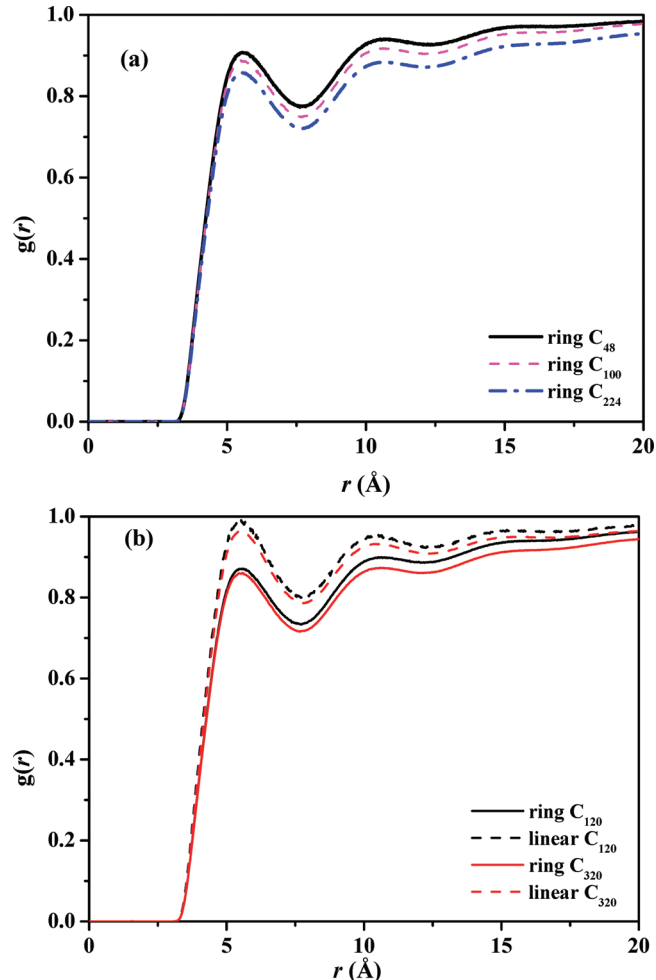


Figure 4. MD simulation results for (a) the intermolecular pair distribution function $g(r)$ of the C_{48} , C_{100} , and C_{224} ring PE systems and (b) the intermolecular pair distribution function $g(r)$ of the C_{120} and C_{320} ring PE systems (solid lines) and their linear analogues (dashed lines).

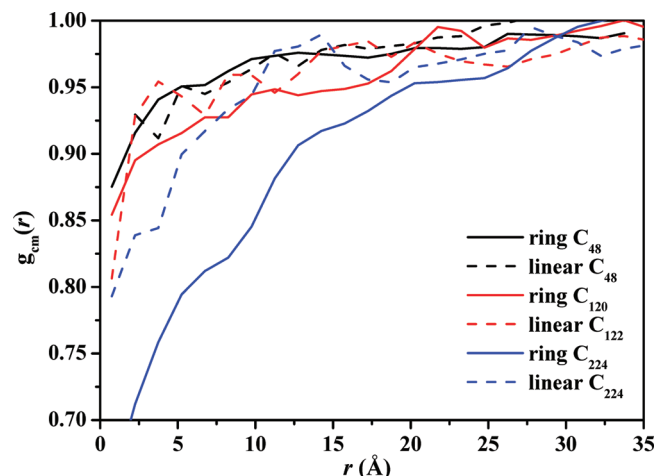


Figure 5. MD simulation results for the chain center-of-mass pair correlation function $g_{cm}(r)$ of the C_{48} , C_{120} , and C_{224} ring PE systems and comparison with the corresponding plots of their linear analogues.

$g_{cm}(r)$, reported in Figure 5: evidently, intermolecular repulsive interactions between rings at the level of entire chains are more pronounced than between linear ones, a phenomenon which becomes more and more evident as the chain length increases.

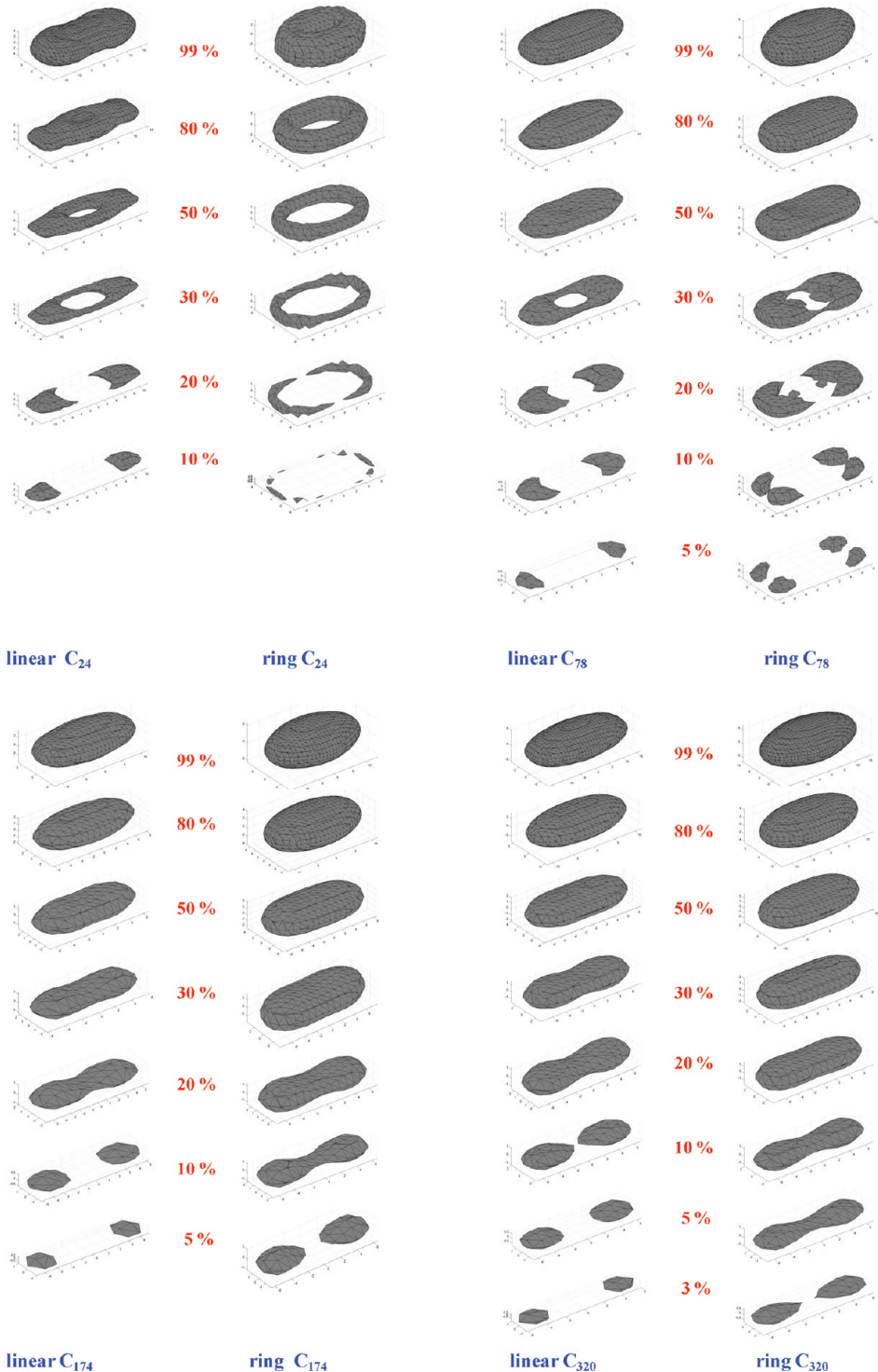


Figure 6. Intrinsic molecular shapes of ring and linear PE chains at $T = 450\text{ K}$ and $P = 1\text{ atm}$.

Intrinsic Molecular Shape. In addition to analyzing structure in polymeric systems at the level of intermolecular pair correlation functions, one can attempt to obtain a picture of the polymeric molecule as an overall object (an organized ensemble of atomistic units) by analyzing the intrinsic molecular shape of this object. To this, one can examine isosurface plots computed at equal values of the average monomer number density in the frame of the principal axes (corresponding to the three eigenvectors) of the instantaneous radius of gyration tensor for each chain. Representative results are shown in Figure 6 where the segment clouds

containing different percentages (3%–99%) of the total number of monomers in a chain are displayed for the two different structures analyzed here, ring and linear. First of all, we note that the intrinsic molecular shape of the linear systems resembles a “cake of soap” instead of an isotropic sphere or ellipsoid, which is fully consistent with the theoretical predictions of Šolc and Stockmayer¹⁰⁰ and the Monte Carlo simulation results of Theodorou and Suter¹⁰¹ for unperturbed polypropylene chains using the rotational isomeric state model. For the molecular shape corresponding to 99% segment density, the present computations reveal that

ring polymers exhibit a more compact disk-like shape than linear polymers, especially for short chain length rings where the overall shape is more round than that of the corresponding linear at the same isosurface density. We also observe that as the value of the segment cloud density increases (from 99% to 3% as we go from top to bottom in Figure 6), the shape of the ring systems (except for the very short ones, e.g., the C₂₄) reveals its two dense cores near the two lobi of highest density at higher segment densities than it is observed for the corresponding linear polymers. This is again a manifestation of the more compact and uniform intramolecular structure of carbon atoms in a ring accompanying their arrangement along a closed loop. As far as the sudden appearance of a hole in the middle of the computed isosurface plots in the case of the very short C₂₄ ring is concerned, this is due to the rather strong tension developing in such very short rings (chains should bend considerably in order to form a closed loop), which enhances bond-bending and bond-torsional interactions. But, clearly, as the chain length increases, the shape of a ring molecule comes closer to that of a linear one, a result which indicates that long enough rings possess (practically) the same degree of chain flexibility as linear ones.

4.2. Dynamical Properties. Local Dynamics. Local dynamics in polymeric systems such as those addressed here (melts of linear and ring PE chains) can be analyzed by computing the torsional autocorrelation function (TACF) of the dihedral angles ϕ along the chain skeleton:

$$P(\phi(t)) = \frac{\langle \cos(\phi(t)) \cos(\phi(0)) \rangle - \langle \cos(\phi(0)) \rangle^2}{\langle \cos(\phi(0)) \cos(\phi(0)) \rangle - \langle \cos(\phi(0)) \rangle^2} \quad (47)$$

Representative results from the present MD simulations with five ring PE systems (C₂₄, C₄₈, C₆₀, C₁₀₀, and C₁₂₀) at T = 450 K are shown in Figure 7a, in a log-linear plot. The results indicate a slightly slower relaxation in the shorter systems, since it is only for chains longer than C₁₂₀ that chain-length independent curves are obtained. In all probability, this is caused by the extra stiffness of their chain structure, which, as the chain length increases, drops gradually and eventually disappears. In Figure 7b, on the other hand, we compare the TACFs of two of the simulated ring PE systems (solid lines) comprising chains with 48 and 120 carbon atoms each to the corresponding ones from the simulations with the linear analogues (dashed lines). For the shorter of the two systems (C₄₈), the segmental dynamics of the ring structure is slower than that of the linear one; in contrast, for the longer system (C₁₂₀), rings and linear chains exhibit practically identical torsional relaxations. Overall, however, and for all practical purposes, we can argue that linear and ring PE melts of the same chain length exhibit very similar torsional relaxations.

In the literature, a common strategy for quantifying local dynamics in polymer melts is to fit the observed decay of the P($\phi(t)$) curves with a stretched exponential Kohlrausch–Williams–Watts (KWW) function of the form:

$$P(\phi(t)) = \exp(-(t/\tau_{KWW}^\phi)^{\beta^\phi}) \quad (48)$$

with τ_{KWW}^ϕ and β^ϕ being the characteristic relaxation time and stretching exponent parameters, respectively. We followed a similar strategy in the present work and the results obtained for the characteristic time τ_{KWW}^ϕ , the stretching exponent β^ϕ , and the correlation time τ_c^ϕ (the integral below the P($\phi(t)$) -vs- t curves) calculated through $\tau_c^\phi = \tau_{KWW}^\phi (\Gamma(1/\beta)/\beta)$ are reported in Table 4. The data confirm that for rings longer in chain

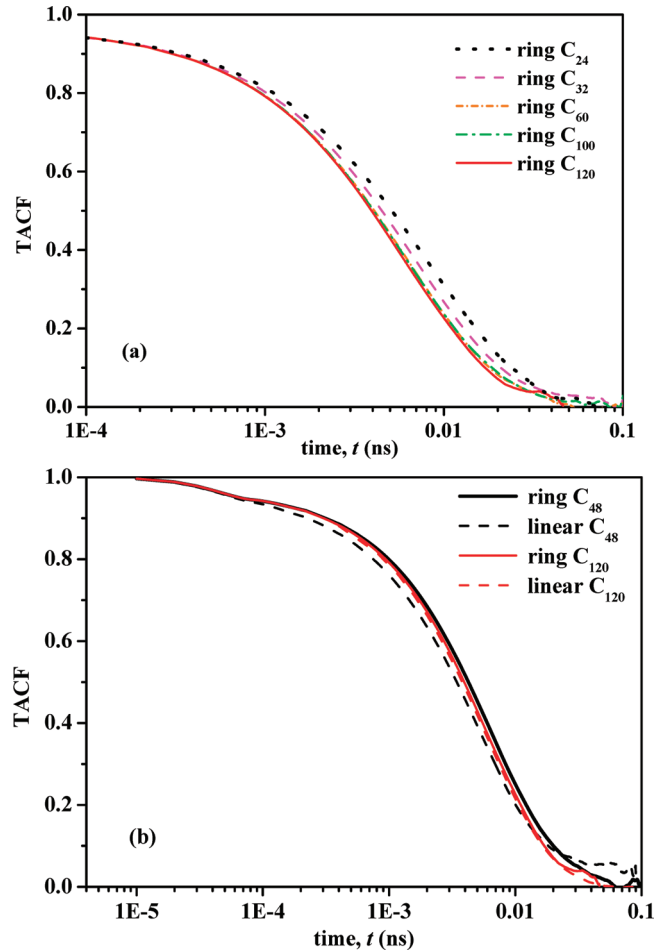


Figure 7. Torsional time autocorrelation function for (a) five of the simulated ring PE systems and (b) the C₄₈ and C₁₂₀ ring PE systems (solid lines) and their linear analogues (dashed lines), in a log–linear plot.

length than C₁₂₀, τ_c^ϕ attains an asymptotic value which for the simulation conditions set here ($T = 450$ K and $P = 1$ atm) is approximately 7 ps. We also observe that the value of the stretching exponent β^ϕ comes out to be approximately the same for all simulated rings (between 0.74 and 0.80 for $T = 450$ K and $P = 1$ atm).

Relaxation Spectrum of the Rouse Modes. The long trajectories accumulated in the course of the MD simulations conducted here can serve as a starting point for testing the range of chain lengths for which the Rouse model version for ring chains provides a reliable description of their dynamics. There are several tests that one can think of: the first is to test eq 14a that the mean squared amplitude $\langle \mathbf{X}_p(0)^2 \rangle$ of the p^{th} Rouse mode scales with N and p as N/p^2 . Results obtained for five of the simulated ring PE systems (C₆₀, C₁₀₀, C₁₇₄, C₃₂₀, and C₄₀₀) are reported in Figure 8. For a given chain length N , the Rouse scaling is seen to be followed only for the lower p modes (more precisely for the modes p for which $N/p^2 > 2$); for higher p modes (i.e., for $N/p^2 < 2$), significant deviations from the Rouse theory are observed for all chain lengths, especially the shorter ones. Our conclusions here seem to parallel those drawn from a similar comparison of atomistic MD simulation data with the corresponding version of the Rouse model for linear polymers (e.g., PE⁹⁹ and 1,4-PB^{102,103}), the deviations being attributed in all cases to the non-Gaussian dynamics of the very short subchains corresponding to rather high p values.¹⁰⁴ A second test of the Rouse model for melts of ring chains refers to the time

Table 4. Values of the Characteristic Relaxation Time τ_{KWW}^ϕ , Stretching Exponent β^ϕ , and Correlation Time τ_c^ϕ of the KWW Function Employed To Fit the MD Simulation Results for the Time Autocorrelation Function of the Torsional Angles ϕ in the Simulated Ring PE Melts ($T = 450$ K, $P = 1$ atm)

system	τ_{KWW}^ϕ (ps)	β^ϕ	τ_c^ϕ (ps)
C ₂₄	8.15	0.77	9.48
C ₃₂	7.10	0.74	8.59
C ₄₈	6.73	0.75	7.99
C ₆₀	6.38	0.79	7.29
C ₁₀₀	6.27	0.77	7.30
C ₁₂₀	6.14	0.79	7.03
C ₁₇₄	6.23	0.80	7.06

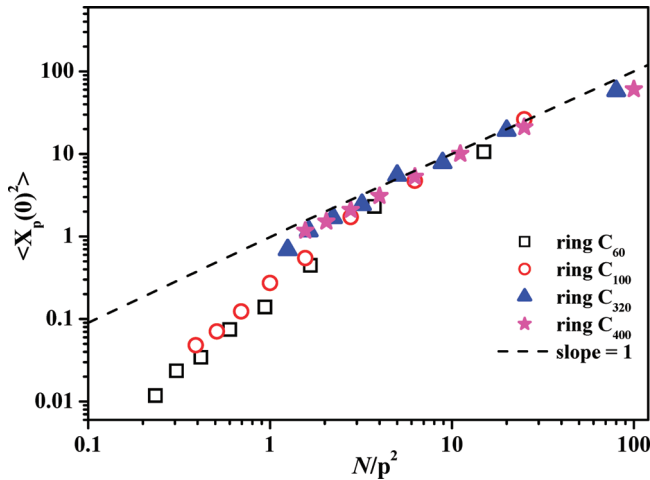


Figure 8. Squared amplitude of the Rouse normal modes $\langle X_p(0)^2 \rangle$ for the C₆₀, C₁₀₀, C₃₂₀, and C₄₀₀ simulated ring PE systems as a function of N/p^2 in a log–log plot.

decay of the normalized autocorrelation function $\langle X_p(t) \cdot X_p(0) \rangle / \langle X_p(0)^2 \rangle$. According to eq 14a, a log–linear plot of $\langle X_p(t) \cdot X_p(0) \rangle / \langle X_p(0)^2 \rangle$ versus $t/(N/p^2)$ should yield a straight line. Numerical results for the relaxation of the first five modes ($p = 2, 4, 6, 8$, and 10) from our MD simulations with the C₁₀₀ and C₁₇₄ ring PE systems are shown in Figure 9, parts a and b. If the rings behaved identically as Rouse chains, all curves should have collapsed onto a single straight line. This is not the case in the data reported in the figure: in all cases, significant deviations from the ideal Rouse behavior are observed, especially for the higher modes. Given that the p th mode probes the dynamics of a subchain of N/p -segments long, these deviations indicate a strong departure of the dynamics of these subchains from the Gaussian behavior, similar to what is already known in the literature for linear unentangled melts.^{99,102,103} It is interesting though that the deviation from the Rouse scaling decreases as the chain length increases.

Since the decay of the $\langle X_p(t) \cdot X_p(0) \rangle / \langle X_p(0)^2 \rangle$ curves cannot be described by a single exponential, we can attempt to fit it with a KWW function (i.e., as we did with the TACFs):

$$\langle X_p(t) \cdot X_p(0) \rangle / \langle X_p(0)^2 \rangle = A(p) \exp \left(- \left(\frac{t}{\tau_{KWW}^p} \right)^{\beta^p} \right) \quad (49)$$

where τ_{KWW}^p and β^p are the characteristic relaxation time and stretching exponent parameters referring to the relaxation of the p th normal mode, respectively, and $A(p)$ the amplitude. The latter is introduced in order to account for the fast decay

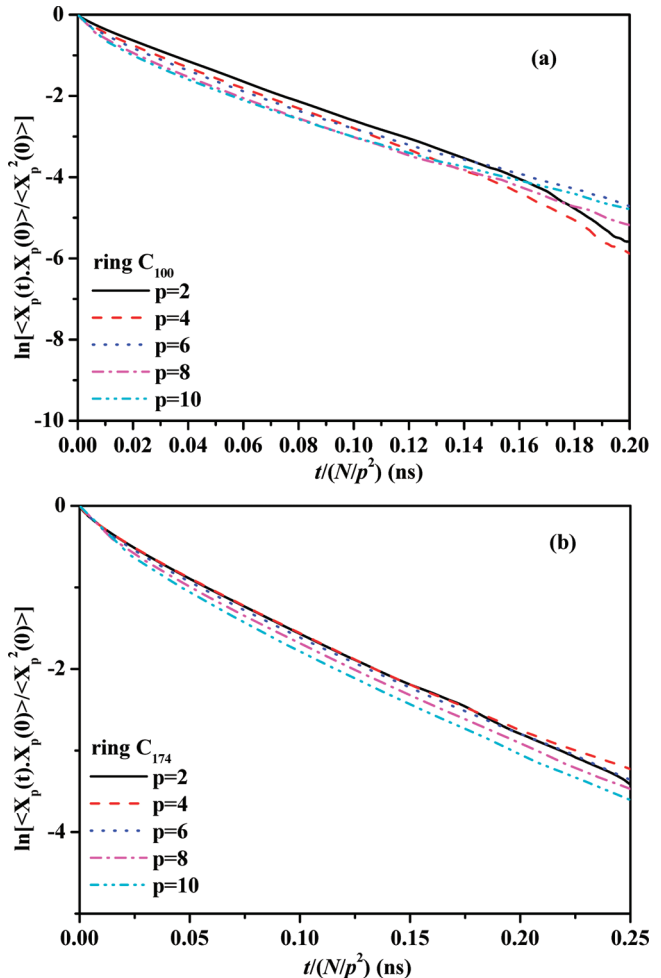


Figure 9. Time autocorrelation functions of the first five normal modes for the (a) C₁₀₀ and (b) C₁₇₄ ring PE systems plotted against $t/(N/p^2)$ in a log–linear plot.

of all normal modes at subpicosecond time scales ($t < 1–2$ ps), and its best-fit value was found to be between 0.8 and 1. The corresponding correlation time is again given by the integral below the corresponding $\langle X_p(t) \cdot X_p(0) \rangle / \langle X_p(0)^2 \rangle$ -vs- t curves and comes out to be:

$$\tau_c^p = \frac{\Gamma\left(\frac{1}{\beta^p}\right)}{\beta^p} \tau_{KWW}^p \quad (50)$$

Figure 10 presents plots of $\tau_p(p\pi/2N)^2$ versus N/p , which, according to the Rouse theory (see eqs 13 and 15), should have fallen on the same straight (horizontal) line. Consistent with the data reported in Figure 9, we see this to be approximately so only for the lower normal modes; higher modes, in contrast, deviate significantly from the Rouse scaling.

Terminal Relaxation Properties. To quantify terminal relaxation in the simulated PE rings we have computed the time decay of the orientational autocorrelation function of the ring diameter vector, $\langle \mathbf{R}_d(t) \cdot \mathbf{R}_d(0) \rangle / \langle R_d^2 \rangle$. According to the Rouse theory, this should follow the scaling described by eq 18. Figure 11 presents the simulation data for two of the PE ring systems studied here (C₁₀₀ and C₁₇₈), alongside with the corresponding Rouse model predictions; the latter have been computed by keeping only the first four terms in the summation in eq 18 and by using the values for the characteristic relaxation times τ_p obtained from the normal-mode

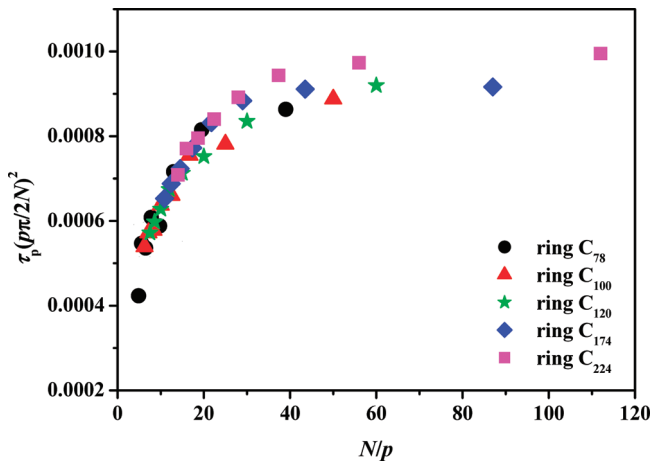


Figure 10. Plots of $\tau_p(p\pi/2N)^2$ versus N/p , for five of the simulated ring PE systems. According to the Rouse theory (eqs 13 and 15), all data should collapse onto a single straight (horizontal) line.

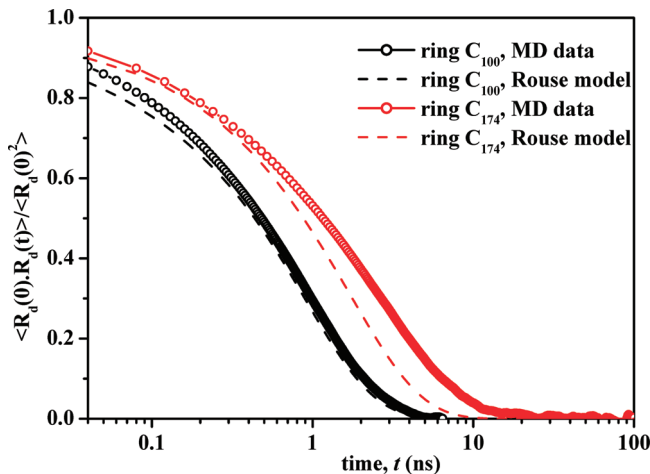


Figure 11. Time autocorrelation function for the ring diameter vector as extracted from the MD simulations with the C_{100} and C_{174} ring PE systems (symbols) and as predicted from the Rouse theory through eq 18 (lines).

analysis discussed in the previous paragraphs (see eqs 49 and 50). For the C_{100} ring PE system, and in contrast to the corresponding behavior of the normal modes, the simulation data for the relaxation of the ring diameter vector are represented by the Rouse model remarkably well. Unfortunately, this is not the case with the C_{174} ring PE system: for this melt, the decay of $\langle \mathbf{R}_d(t) \cdot \mathbf{R}_d(0) \rangle / \langle \mathbf{R}_d^2 \rangle$ exhibits rather significant deviations from the Rouse scaling. The fact that $\langle \mathbf{R}_d(t) \cdot \mathbf{R}_d(0) \rangle / \langle \mathbf{R}_d^2 \rangle$ relaxes considerably slower than what is predicted by the Rouse model for this system makes us suspect non-negligible contributions to its dynamics from mechanisms other than Rouse relaxation, such as architectural restrictions between neighboring or overlapping chains.

Once more, and similar to local dynamics, a more satisfactory description of the $\langle \mathbf{R}_d(t) \cdot \mathbf{R}_d(0) \rangle / \langle \mathbf{R}_d^2 \rangle$ -vs- t curves is offered by a KWW-type of function. Then, from the best-fit values of the corresponding τ_{KWW}^d and β^d parameters, the correlation times τ_d describing terminal relaxation in the studied PE ring melts can be calculated. We have carried out such an analysis and the results are reported in Figure 12, where we examine the dependence of the terminal relaxation time τ_d on chain length N . As shown in the figure (see inset), and for $N \geq 48$, τ_d follows a power law dependence on N of

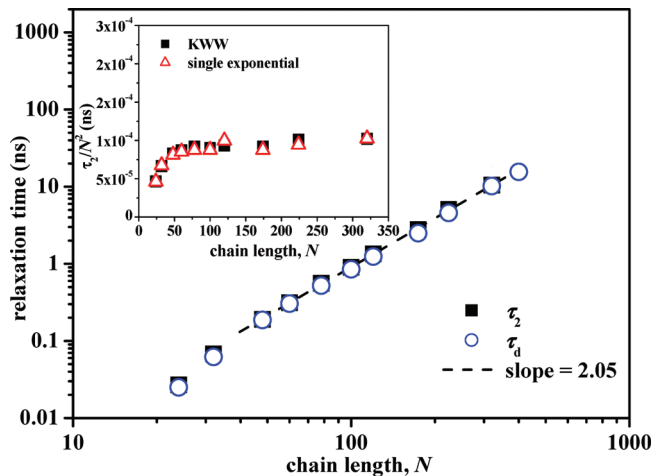


Figure 12. Chain length dependence of the terminal relaxation time as calculated from the time autocorrelation function of the ring diameter vector (open symbols), and of the normal mode $p = 2$ (filled symbols), in a log–log plot. Dashed lines represent the best linear fits to the simulation data.

the form $\tau_d \sim N^{2.05 \pm 0.05}$, a result which seems to agree with eq 15 of the Rouse theory. But the most interesting point here is that, in contrast to linear chains where the Rouse scalings are usually valid over a limited range of chain lengths (for PE, for example, this extends from C_{60} to C_{156}),¹⁰⁵ the corresponding Rouse scalings for ring melts are valid over a significantly broader range of chain lengths. For example, the Rouse scaling that $\tau_d \sim N^{2.05 \pm 0.05}$ holds even for rings with a chain length as long as C_{400} . This is an important difference between rings and linear chains as far as their Rouse behavior is concerned. And it seems to indicate that the characteristic entanglement length for rings is longer than for linear polymers of the same chemical composition, as has already been conjectured in the literature on the basis of a few experimental measurements.^{39,40,59}

Segmental Mean Square Displacement. Analyzing MD simulation trajectories to obtain the mean square displacement (msd) of atomistic segments as a function of time is absolutely important because the results can be used as input to known equations of neutron scattering to compute the dynamic structure factor of the simulated melts (see also later in this paper). Figure 13a presents simulation results for the msd of ring segments $g(t)$ versus time t for four of the ring PE systems simulated here (C_{48} , C_{78} , C_{120} , and C_{224}), in a log–log plot. The curves shown in the figure prove that all ring melts show a typical Rouse-like behavior: for short times, $g(t)$ scales with t as $g(t) \sim t^{0.52 \pm 0.03}$ while at longer times where the Fickian regime is reached $g(t) \sim t^1$. We also see that the time at which the slope of the segmental msd curve exhibits the characteristic break from the value of 0.5 to the value of 1 (this coincides approximately with the corresponding Rouse time) increases with increasing chain length. Figure 13b, on the other hand, displays the computed $g(t)$ curves for two of the PE ring systems simulated here (C_{174} and C_{400}); for the purposes of comparison, also included in the same graph are the computed segmental msd curves from additional MD simulations with the corresponding linear analogues. For both chain lengths, the ring system exhibits a faster dynamics at long time scales than the corresponding linear one, indicating a higher mobility of segments in melts of ring than in melts of linear chains (see also Figure 15). A particularly noticeable feature in the data of Figure 13b is that, for the C_{400} melt, the linear polymer exhibits the three characteristic breaks typical of

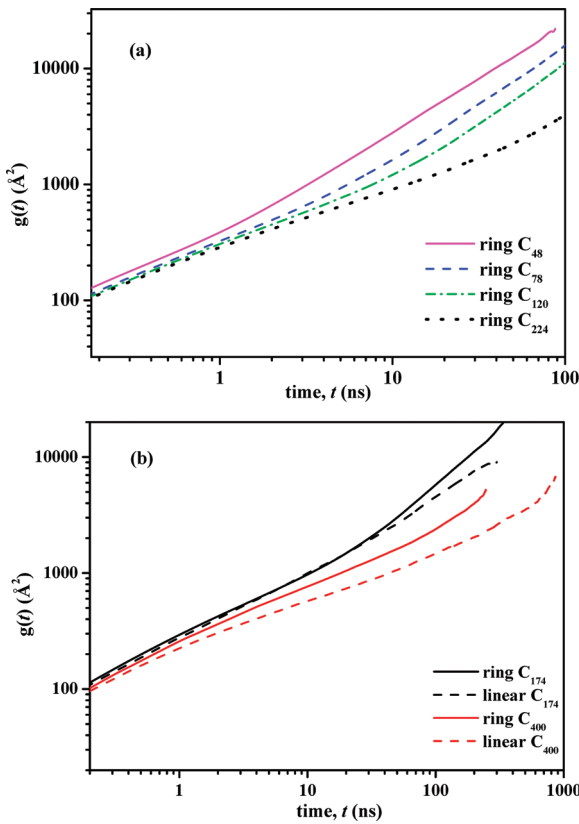


Figure 13. (a) Mean-square displacement of the innermost chain segments versus time for the C_{48} , C_{78} , C_{120} , and C_{224} ring PE systems. (b) Mean-square displacement of the innermost chain segments versus time for the C_{174} and C_{400} ring PE systems (solid lines) and comparison with the corresponding MD simulation results with the linear analogues (dashed lines).

the reptation-like dynamics,⁹ in contrast, the ring one continues to display only one break characteristic of an approximately Rouse-like behavior. This corroborates once more our conjecture that the Rouse scaling in ring melts holds over a more extended range of chain lengths than in linear polymers.

Self-Diffusion Coefficient. Figure 14 presents results for the chain length dependence of the chain center-of-mass self-diffusion coefficient D_G of ring and linear PE systems. The data have been obtained by examining first the mean square displacement of the chain center-of-mass in the two cases and by invoking then the Einstein relationship to compute D_G from the long time scale of the plot where Fickian diffusion is established (see eq 24). Our simulation data indicate that for short chain lengths ($N < 50$), ring PE systems exhibit a slower center-of-mass diffusivity than linear analogues; this is attributed to the higher density of the ring melts (see also Figure 2). The same behavior has been observed in the pulsed-gradient spin-echo nuclear magnetic resonance (PGSE NMR) experiments of von Meerwall et al.⁴⁸ As the chain length increases, however, a crossover is observed at around $N \approx 50$, above which the chain center-of-mass diffusivity of the rings becomes faster than that of the linear analogues. A similar crossover in the D_G -vs- N plots between linear and ring melts from molecular simulations has been reported by Hur et al.²⁷ and Ozisik et al.⁴⁷ On the basis of the findings of our atomistic MD simulations, chain dynamics in ring PE melts with chain length $N \geq 50$ is described quite accurately by a power law of the form $D_G \sim M^{-b}$ with $b = 1.1\text{--}1.3$. Such a scaling which covers PE rings as long as C_{400} is in favor of our argument that ring melts obey Rouse

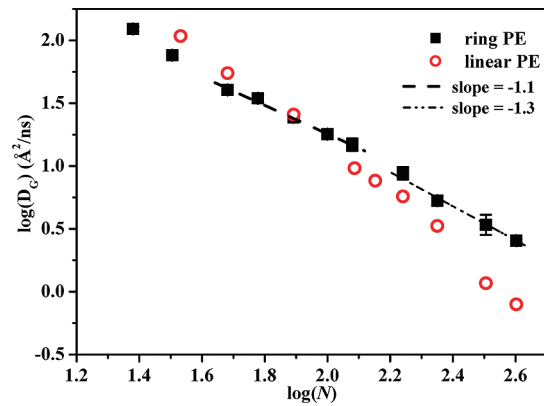


Figure 14. Chain length dependence of the chain center-of-mass self-diffusion coefficient D_G of the simulated ring (filled symbols) and linear (open symbols) PE melts, in a log-log plot.

dynamics over a more extended range of chain lengths than it is known for linear melts (see, e.g., Harmandaris et al.¹⁰⁵ and also the data in Figure 14 referring to linear PE systems where the corresponding crossover from the Rouse to the reptation dynamics characterized by a scaling of the form $D_G \sim M^{-2.4}$ is observed to take place at around C_{156}). Qualitatively similar findings have been observed in other simulation studies.²⁷

Friction Coefficient. A very important parameter that can be extracted indirectly from our atomistic MD simulations (by mapping predictions for certain observables onto the Rouse model) is the segmental (monomeric) friction coefficient ξ . In fact, following Harmandaris et al.^{99,105} and Tsouli et al.,¹⁰² ξ can be obtained by two different mapping schemes: the first utilizes the MD predictions for the chain center-of-mass self-diffusion coefficient to compute ξ through eq 24 of the Rouse model, namely $\xi = k_B T / ND_G$; the resulting value of ξ is denoted as ξ_D . The second is based on the MD results for the longest relaxation time τ_2 of the studied PE rings and computes ξ through eq 15 of the Rouse model, namely $\xi = 3\pi^2 k_B T \tau_2 / N(R_d^2)$; the resulting value of ξ is denoted as ξ_{τ_2} . Results from the two mapping schemes for ξ as a function of the chain length N are reported in Figure 15a. The first observation to make in the numerical data of Figure 15a is that the two methodologies produce quantitatively very similar (i.e., consistent) results for ξ . The second observation is that the extracted ξ values are in magnitude close to the ones reported previously⁹⁹ for unentangled linear PE melts. But the most interesting point in the data of Figure 15a is that the value of ξ is nearly constant for all chain lengths between C_{50} and C_{400} (although a small increase is discernible in the figure as the ring length increases above approximately C_{170}). Again, this result is in support of the validity of the Rouse theory over the entire range of molecular lengths investigated in this work (up to C_{400}), since the theory relies on the consideration of a chain length independent value for the friction coefficient ξ (ξ should depend only on the chemical structure and molecular architecture of the polymer and not on its chain length N).

How exactly the values of the friction coefficient ξ compare between ring and linear PE systems^{99,105} of the same chain length N is analyzed in Figure 15b. To be as more consistent as possible in our comparison, the two sets of values have been extracted from the simulation data for D_G and not for the relaxation time τ_2 because the former are computed directly from the MD simulations whereas the latter require the intermediate fitting to the KWW function. The comparison shows that for $N < 50$, ring melts are

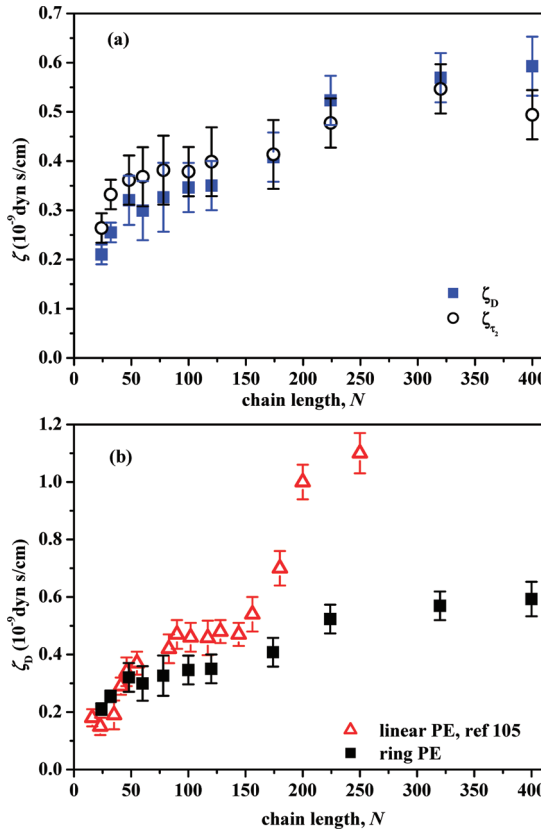


Figure 15. (a) Chain length dependence of the monomeric friction coefficient ζ_D and ζ_{r2} for the simulated ring PE systems as calculated from eqs 24 and 15, respectively. (b) Values of the monomeric friction coefficient ζ_D of the simulated ring PE systems and comparison with the reported values (see ref 105) for the corresponding linear analogues.

characterized by larger ζ_D values than linear melts, reflecting the slower dynamics of the ring chains in this regime of chain lengths (a direct consequence of the higher density of the ring melts due to absence of chain ends). Clearly this is fully consistent with the results for D_G presented in Figure 14. For $N > 50$, on the other hand, ring melts are characterized by smaller ζ_D values than linear analogues; this is a direct consequence of the faster dynamics of ring chains compared to linear ones as the chain length increases which has also been reflected in the values of D_G themselves in the two different types of melts. We also mention that in the interval $50 < N < 150$ both ring and linear systems are characterized by constant (although different) ζ_D values, in accordance with the Rouse theory. The most significant difference between the two systems is again in their behavior for chain lengths above approximately C_{156} : for the linear melts, this is accompanied by a dramatic increase in the value of ζ_D which is a direct consequence of the onset of entanglements and of the passage to the reptation-like type of dynamics. For the rings, on the other hand, ζ_D continues to have the (approximately) same value even for chain lengths as long as C_{400} (the longest PE ring melt simulated here) which we take as an additional evidence that for this category of melts, the Rouse dynamics extends over a significantly broader regime of chain lengths.

Zero-Shear Rate Viscosity. In addition to the friction coefficient ζ , in practical applications of polymeric materials (e.g., in polymer processing operations) one is interested also in the viscosity of the system, especially in its value at small shear rates (known as the zero shear rate viscosity η_0) and its scaling with chain length N . From a statistical mechanics point of view, η_0 can be formally obtained by resorting to the

corresponding Green-Kubo equation for the calculation of the shear modulus of relaxation of the melt.⁹ Since such a direct method suffers from the large statistical noise accompanying the calculation of the off-diagonal components of the stress tensor under equilibrium conditions, one usually resorts to an indirect calculation of η_0 . Harmandaris et al.^{99,105} for example, proposed computing η_0 by mapping atomistic MD data onto the Rouse model for chain lengths below the entanglement chain length N_e , and onto the reptation (or tube) model for chain lengths above N_e , with remarkable success for linear PE and linear *cis*-1,4-PB melts.^{99,102,105,106} We extend the Harmandaris et al.^{99,105} approach here to compute the zero shear rate viscosity of ring PE melts. To this, by combining eqs 15, 24 and 30 and using that $\langle R_d^2 \rangle = Nb^2/4$, we find the following two analytical and equivalent expressions of the Rouse model for η_0 :

$$\eta_0 = \frac{\pi^2 \rho RT}{6 M} \tau_2 \quad (51a)$$

$$\eta_0 = \frac{\rho RT}{18 D_G M} \langle R_d^2 \rangle \quad (51b)$$

where M denotes the molecular weight of the simulated melt, ρ its mass density, and R the gas constant. Since the values of D_G , $\langle R_d^2 \rangle$, and τ_2 are already known from our MD simulations, eqs 51a and 51b provide a rather straightforward way for estimating η_0 . We consider this as an *indirect* way for obtaining η_0 for unentangled melts of polymeric rings, since it combines atomistic MD simulation data with elements of the Rouse theory. Representative results from such an approach are displayed in parts a and b of Figure 16. Our numerical data are seen to be internally consistent for all chain lengths, especially for the systems with $N > 48$ where they seem to confirm the Rouse scaling, namely that $\eta_0 \sim M^1$ (represented by the dashed line in Figure 16a). Figure 16b, on the other hand, shows how the values of η_0 differ between ring and linear PE melts^{105–109} of the same chain length N . The conclusion is that ring PE melts are characterized by η_0 values that are systematically smaller than those of their linear analogues. Furthermore, as the chain length increases, their difference becomes larger and larger: for example, the ratio $\eta_{0,\text{ring}}/\eta_{0,\text{linear}}$ of the two viscosities is approximately equal to 0.2–0.3 for $N < 60$ but increases rapidly to about 0.5 for intermediate chain lengths ($78 < N < 120$), exactly as predicted by the Rouse model (see text below eq 30). For even longer PE melts, the ratio is seen to decrease dramatically, a behavior which we should have expected given that the zero shear rate viscosity of the corresponding linear analogues increases sharply above approximately C_{156} as these systems cross over to the reptation dynamics. In contrast, the viscosity of the corresponding ring PE melts exhibits a smoother change with N even for ring chains as long as C_{400} , thus continuing to follow approximately the Rouse scaling.

Dynamic Structure Factor. As already mentioned above, dynamics in polymers is experimentally probed by neutron scattering (NS) and neutron spin echo (NSE) experiments through measurements of the single-chain dynamic structure factor $S(\mathbf{q}, t)$, defined by eq 35. In fact, by analyzing the measured $S(\mathbf{q}, t)$ spectra on the basis of the predictions of the two very successful molecular theories for polymers (Rouse and reptation) leads to invaluable information about their dynamics as a function of chain length. This happens because by varying the magnitude q of the scattering vector \mathbf{q} one can explore the entire spectrum of relaxation times for a given

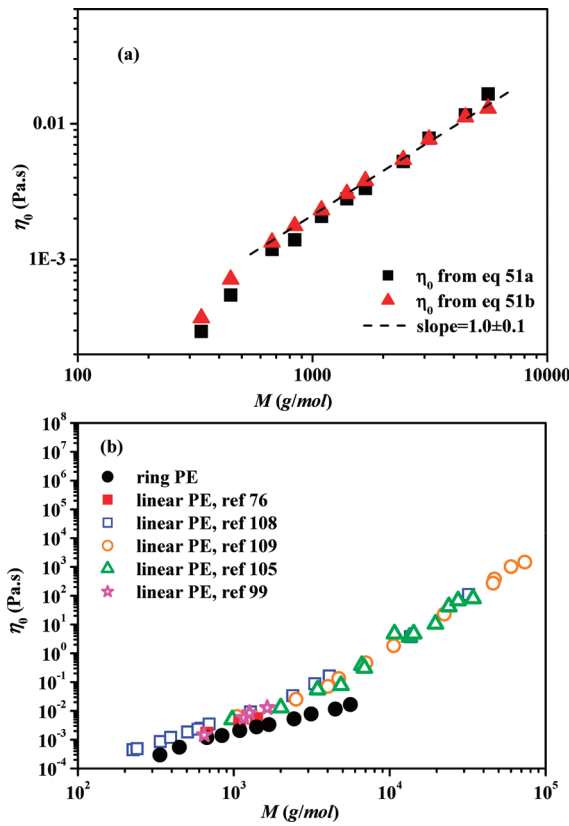


Figure 16. (a) Molecular weight dependence of the zero shear rate viscosity η_0 of the simulated ring PE systems as calculated indirectly from the MD simulations with the help of eqs 51a (squares) and 51b (triangles), in a log–log plot. (b) Computed zero shear rate viscosity η_0 values for the simulated ring PE systems and comparison with available (simulation and experimental) data for linear PE analogues.

polymer: small q values (e.g., $0.01 \leq q \leq 0.1 \text{ \AA}^{-1}$) to probe relaxation at the level of entire chains (terminal relaxation) and large q values (e.g., $1.0 \leq q \leq 5.0 \text{ \AA}^{-1}$) to probe relaxation at shorter length scales (segmental or local dynamics).

Representative results from our MD simulations for the dynamic structure factor of the simulated ring PE melts are shown in Figure 17. Actually, what we report in the figure is the normalized single-chain coherent dynamic structure factor $S'(q,t)$

$$S'(q,t) = \frac{S(q,t)}{S(q,0)} = \frac{\sum_{n,m} \langle \sin[qR_{nm}(t)]/qR_{nm}(t) \rangle}{\sum_{n,m} \langle \sin[qR_{nm}(0)]/qR_{nm}(0) \rangle} \quad (52)$$

for several of the simulated ring PE systems (C_{60} , C_{100} , and C_{174}), at different q values (in eq 52, $R_{nm} = |\mathbf{R}_n(t) - \mathbf{R}_m(0)|$). Also shown in the figure are the predictions of the Rouse model through a direct application of eqs 35–37. The Rouse theory is found to offer an excellent description of the simulation data for almost all q values examined in Figure 17, even for the longer C_{320} system. It is only for the very high q value ($= 0.2 \text{ \AA}^{-1}$ in Figure 17b) for the C_{100} ring PE system that the Rouse model predicts a somewhat faster decay of the $S'(q,t)$ curve compared to the simulation data. A similar inadequacy of the Rouse model to follow the $S'(q,t)$ spectrum at large q values is also known for unentangled linear polymer melts (both from simulation studies and experimental observations), and it is typically attributed to the non-Gaussian character of the segmental displacements corresponding to large wavevectors.^{102–105}

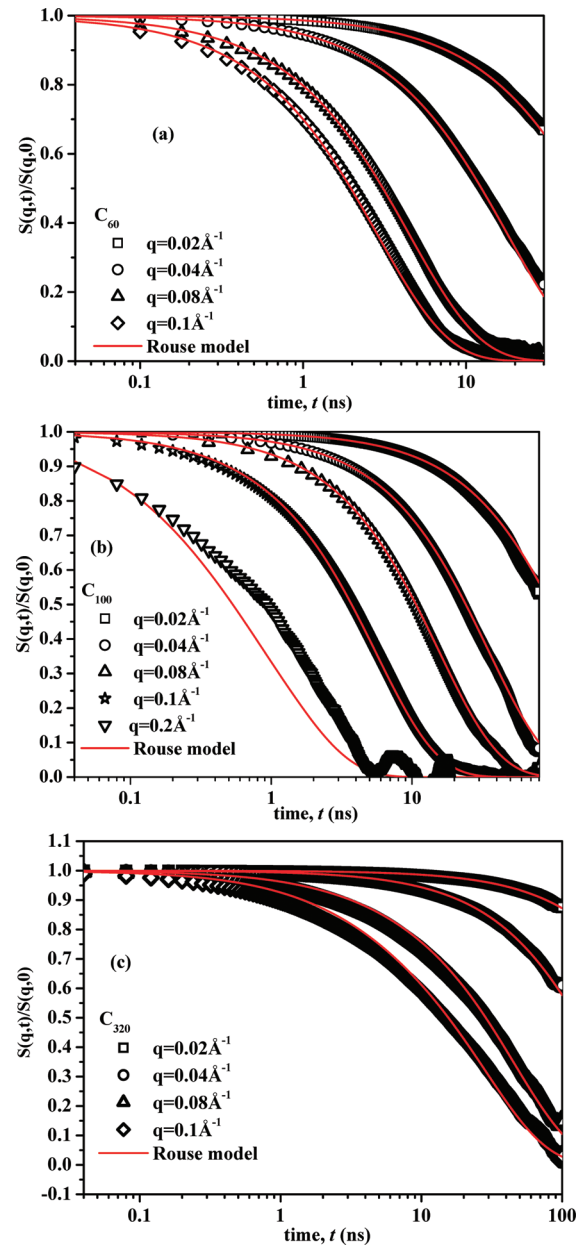


Figure 17. Plots of the normalized single-chain dynamic structure factor $S(q,t)/S(q,0)$ as obtained directly from the atomistic MD simulations with the (a) C_{60} , (b) C_{100} and (c) C_{320} ring PE systems, for several q values. Solid lines represent the corresponding Rouse model predictions from eqs 35–37.

5. Conclusions and Future Plans

We have presented a thorough analysis of the structural, dynamical, and viscoelastic properties of unentangled melts of PE rings through large-scale atomistic MD simulations for a number of systems ranging in chain length from C_{24} up to C_{400} . We have also provided a detailed and rather comprehensive analysis of the Rouse model for these systems at both the continuum (section 2) and discrete (Appendix) levels, and we have extensively discussed its predictions for the structural and linear rheological properties, with emphasis on their scaling with chain length. Consistent with previous works, our results about the radius of gyration, packing length, pair correlation function, and intrinsic molecular shape of the chains have revealed and demonstrated the more compact and symmetric structure of ring chains in their molten state compared to their linear analogues. This more compact structure (shrinkage) of ring chains in melt has its

source to the architectural restrictions accompanying chain non-concatenation, which creates an effective pressure that tends to squeeze neighboring ring chains one against another. On the basis of this picture, one should expect that the degree of shrinkage will increase with increasing chain length, which is exactly consistent with the results of our work (see, e.g., Figure 1). For ring melts with $N > 120$, our simulations are in support of the scaling $R_g \sim N^{0.45 \pm 0.02}$ for the ring radius of gyration. Additional calculations of the intermolecular mer-mer and center-of-mass pair correlation functions have revealed a correlation hole effect which is more pronounced (the hole is deeper) in the ring PE system than in the corresponding linear with the same chain length.

Our MD simulation results for local dynamics (based on the decay of the TACF) indicate a somewhat slower relaxation in the shorter-chain systems which, however, tends to saturate for long enough chains (chains longer than C_{120}); this has been attributed to the stiffer structure of shorter rings, since a short chain has to bend considerably in order to fold back to itself and close the loop. We have further seen that the proposed Rouse theory offers overall a satisfactory description of the rheological behavior of the simulated melts. Dynamical properties analyzed here included a variety of observables (some of them also directly accessible experimentally): the segmental msd, the chain center-of-mass self-diffusion coefficient D_G , the terminal relaxation time τ_d from the time decay of $\langle \mathbf{R}_d(t) \cdot \mathbf{R}_d(0) \rangle / \langle \mathbf{R}_d^2 \rangle$, the characteristic spectrum of the Rouse relaxation times τ_p from the time decay of $\langle \mathbf{X}_p(t) \cdot \mathbf{X}_p(0) \rangle / \langle \mathbf{X}_p^2(0) \rangle$, and the single-chain dynamic structure factor $S(\mathbf{q}, t)$. We have also provided reliable estimates of two important rheological parameters of the simulated ring PE melts, the fiction coefficient ξ and the zero-shear rate viscosity η_0 , by utilizing a consistent mapping of the MD simulation data onto the corresponding Rouse model.

We close by noting that the observed persistence of Rouse-like dynamics for rings with the chain length might be attributed (at least in part) to the relatively weaker dependency of their scaling behavior on chain length as compared to linear polymers. Thus, atomistic MD simulations with longer PE rings are currently in progress to elucidate this issue further and completely understand system behavior in the transition zone from the Rouse to the entangled regime. Trajectories accumulated in the course of these MD simulations with longer ring melts will also serve as input in a subsequent topological analysis aiming at revealing the nature of topological interactions behind their unique rheological properties as their chain length increases above a characteristic value.

Acknowledgment. The authors would like to acknowledge financial support from the DYNACOP European Project (FP7-PEOPLE-2007-1-1-ITN). They also feel deeply indebted to Prof. Dimitris Vlassopoulos and Dr. Wim Pyckhout-Hintzen for many useful discussions in the course of this work.

Appendix. Discrete Rouse Model for Ring Polymers

In this Appendix we provide a detailed analysis of the discrete Rouse model for ring polymers. Initially, to gain some insight into the dynamics of these systems (also to understand how this compares to that of linear analogues), we present an analysis of the characteristic eigenvalues and eigenvectors of bead dynamics for a few short ring (and linear) chains. The results are generalized next for rings of arbitrary chain length.

We start our analysis by writing down the Langevin equation for the vector \mathbf{R} defined as $\mathbf{R} = [\mathbf{R}_1, \mathbf{R}_2, \mathbf{R}_3, \dots, \mathbf{R}_N]^T$ (the superscript T denotes the transpose) in the following form

$$\frac{d\mathbf{R}}{dt} = -\frac{K}{\xi} \mathbf{A} \mathbf{R} \quad (A1)$$

i.e., by neglecting the random forces \mathbf{f}_n , since these are irrelevant for the computation of the characteristic eigenvalues and

eigenvectors (see eqs 1 and 2). For both linear and ring polymers, \mathbf{A} is a real, symmetric matrix, thus all of its eigenvalues will be real with the corresponding eigenvectors orthogonal to each other.¹¹⁰

(i). Linear and Ring Chains with $N = 3$. In this case, the matrix \mathbf{A} is given by

$$\mathbf{A} = \begin{bmatrix} 1 & -1 & 0 \\ -1 & 2 & -1 \\ 0 & -1 & 1 \end{bmatrix} \text{ for a linear chain, and}$$

$$\mathbf{A} = \begin{bmatrix} 2 & -1 & -1 \\ -1 & 2 & -1 \\ -1 & -1 & 2 \end{bmatrix} \text{ for a ring chain} \quad (A2)$$

Solving $|\lambda\mathbf{I} - \mathbf{A}| = 0$, we obtain the following sets of eigenvalues: $\{\lambda_0, \lambda_1, \lambda_2\} = \{0, 1, 3\}$ for the linear chain, and $\{\lambda_0, \lambda_2\} = \{0, 3\}$ for the ring chain with $\lambda_2 (= 3)$ having a multiplicity of 2. The eigenvalues for the linear chain are in full agreement with the known general formula $\lambda_p = 4 \sin^2(p\pi/2N)$ for $p = 0, 1, 2, 3, \dots, N-1$. The following points are in order here: (a) no eigenvalues corresponding to odd p modes (i.e., the λ_1) exist for rings, (b) the eigenvalues corresponding to even p modes (including $p = 0$) are the same between linear and ring chains, (c) the eigenvectors corresponding to even p modes are different between linear and ring chains, reflecting different relaxation mechanisms for beads in the two cases, and (d) the $p = 0$ eigenvalue (i.e., λ_0) is equal to zero both for linear and ring chains; this holds for all chain lengths since \mathbf{A} is singular (i.e., $|\mathbf{A}| = 0$); the corresponding (normalized) eigenvector ξ_0 is given by $(1/\sqrt{N})[1, 1, \dots, 1]^T$ for an N -bead chain representing physically a uniform translation of the entire chain in space. We conclude this preliminary analysis by reporting that for $N = 3$ the other eigenvectors are

$$\xi_1 = [1/\sqrt{2}, 0, -1/\sqrt{2}]^T$$

and

$$\xi_2 = [1/\sqrt{6}, -\sqrt{6}/3, 1/\sqrt{6}]^T$$

for a linear chain, and

$$\xi_2 = [1/\sqrt{2}, 0, -1/\sqrt{2}]^T$$

and $[1/\sqrt{2}, -1/\sqrt{2}, 0]^T$ for a ring chain. The forms of the two eigenvectors point to characteristic bead motions that are different in the two chains.

(ii). Linear and Ring Chains with $N = 4$. Here

$$\mathbf{A} = \begin{bmatrix} 1 & -1 & 0 & 0 \\ -1 & 2 & -1 & 0 \\ 0 & -1 & 2 & -1 \\ 0 & 0 & -1 & 1 \end{bmatrix} \text{ for a linear chain, and}$$

$$\mathbf{A} = \begin{bmatrix} 2 & -1 & 0 & -1 \\ -1 & 2 & -1 & 0 \\ 0 & -1 & 2 & -1 \\ -1 & 0 & -1 & 2 \end{bmatrix} \text{ for a ring chain} \quad (A3)$$

The four eigenvalues are then $\{\lambda_0, \lambda_1, \lambda_2, \lambda_3\} = \{0, 2 - \sqrt{2}, 2, 2 + \sqrt{2}\}$ for the linear chain (which is again consistent with the known analytical result that $\lambda_p = 4\sin^2(p\pi/2N)$) and $\{\lambda_0, \lambda_2, \lambda_4\} = \{0, 2, 4\}$ for the ring chain ($\lambda_2 = 2$ has again a multiplicity of 2). No eigenvalue with an odd p mode (e.g., λ_1 or λ_3) exists for the ring chain. We also see that the second eigenvalue (λ_2) is the same in the two chains (linear and ring) but the corresponding eigenvectors are different: $\xi_2 = (1/2)[1, -1, -1, 1]^T$ for the linear chain, and

$$\xi_2 = [1/\sqrt{2}, 0, -1/\sqrt{2}, 0]^T$$

and $[0, 1/\sqrt{2}, 0, -1/\sqrt{2}]^T$ for the ring chain.

(iii). Linear and Ring Chains with $N = 5$. Here

$$\mathbf{A} = \begin{bmatrix} 1 & -1 & 0 & 0 & 0 \\ -1 & 2 & -1 & 0 & 0 \\ 0 & -1 & 2 & -1 & 0 \\ 0 & 0 & -1 & 2 & -1 \\ 0 & 0 & 0 & -1 & 1 \end{bmatrix}$$

for a linear chain, and

$$\mathbf{A} = \begin{bmatrix} 2 & -1 & 0 & 0 & -1 \\ -1 & 2 & -1 & 0 & 0 \\ 0 & -1 & 2 & -1 & 0 \\ 0 & 0 & -1 & 2 & -1 \\ -1 & 0 & 0 & -1 & 2 \end{bmatrix}$$

for a ring chain

(A4)

Working in exactly the same way, we find that

$$\{\lambda_0, \lambda_1, \lambda_2, \lambda_3, \lambda_4\} = \left\{ 0, 4\sin^2\left(\frac{\pi}{10}\right), 4\sin^2\left(\frac{\pi}{5}\right), 4\sin^2\left(\frac{3\pi}{10}\right), 4\sin^2\left(\frac{2\pi}{5}\right) \right\}$$

for a linear chain and

$$\{\lambda_0, \lambda_2, \lambda_4\} = \left\{ 0, 4\sin^2\left(\frac{\pi}{5}\right), 4\sin^2\left(\frac{2\pi}{5}\right) \right\}$$

for a ring chain. We confirm again that (a) the eigenvalues of the even p modes (λ_2 and λ_4) are the same between the two chains and (b) no eigenvalue with odd p number exists for the ring chain.

On the basis of the above preliminary results for $N = 3, 4$, and 5 , we conclude therefore that: (a) ring chains do not possess eigenvalues with odd p modes, and (b) the eigenvalues corresponding to even p modes are the same between linear and ring chains of the same chain length. This implies that the known general formula $\lambda_p = 4\sin^2(p\pi/2N)$ with $p = 0, 1, 2, 3, \dots, N-1$ for the eigenvalues of an N -bead linear chain should also describe the eigenvalues of the corresponding ring chain, but only for even p modes (i.e., $p = 0, 2, 4, \dots, N$). These conjectures are analytically verified below.

(iv). General Formula for the Eigenvalues and Eigenvectors for Ring Polymers. For an arbitrary N -bead long polymeric

chain, the matrix \mathbf{A} has the form:

$$\mathbf{A} = \begin{bmatrix} 1 & -1 & 0 & 0 & \cdots & 0 & 0 & 0 & 0 \\ -1 & 2 & -1 & 0 & \cdots & 0 & 0 & 0 & 0 \\ 0 & -1 & 2 & -1 & \cdots & 0 & 0 & 0 & 0 \\ 0 & 0 & -1 & 2 & \cdots & 0 & 0 & 0 & 0 \\ \vdots & \vdots & \vdots & \vdots & \ddots & \vdots & \vdots & \vdots & \vdots \\ 0 & 0 & 0 & 0 & \cdots & 2 & -1 & 0 & 0 \\ 0 & 0 & 0 & 0 & \cdots & -1 & 2 & -1 & 0 \\ 0 & 0 & 0 & 0 & \cdots & 0 & -1 & 2 & -1 \\ 0 & 0 & 0 & 0 & \cdots & 0 & 0 & -1 & 1 \end{bmatrix}$$

for a linear chain

(A5a)

$$\mathbf{A} = \begin{bmatrix} 2 & -1 & 0 & 0 & \cdots & 0 & 0 & 0 & -1 \\ -1 & 2 & -1 & 0 & \cdots & 0 & 0 & 0 & 0 \\ 0 & -1 & 2 & -1 & \cdots & 0 & 0 & 0 & 0 \\ 0 & 0 & -1 & 2 & \cdots & 0 & 0 & 0 & 0 \\ \vdots & \vdots & \vdots & \vdots & \ddots & \vdots & \vdots & \vdots & \vdots \\ 0 & 0 & 0 & 0 & \cdots & 2 & -1 & 0 & 0 \\ 0 & 0 & 0 & 0 & \cdots & -1 & 2 & -1 & 0 \\ 0 & 0 & 0 & 0 & \cdots & 0 & -1 & 2 & -1 \\ -1 & 0 & 0 & 0 & \cdots & 0 & 0 & -1 & 2 \end{bmatrix}$$

for a ring chain

(A5b)

To calculate their eigenvalues, we note from eq A5a that for a linear chain the following recursive relation of the secular equation applies:¹¹¹

$$|\lambda\mathbf{I} - \mathbf{A}|_N^{linear} = (\lambda - 2)|\lambda\mathbf{I} - \mathbf{A}|_{(N-1)}^{linear} - |\lambda\mathbf{I} - \mathbf{A}|_{N-2}^{linear} \quad (A6)$$

In the case of a ring chain, instead of a recursive relation in itself, one can make use of the following relation in terms of the secular equations of the corresponding N - and $(N-1)$ -bead long linear chains:

$$|\lambda\mathbf{I} - \mathbf{A}|_N^{ring} = (\lambda - 2)|\lambda\mathbf{I} - \mathbf{A}|_N'^{linear} - 2\left[|\lambda\mathbf{I} - \mathbf{A}|_{N-1}'^{linear} + (-1)^N\right] \quad (A7a)$$

or, equivalently

$$|\lambda\mathbf{I} - \mathbf{A}|_N^{ring} = \left[(\lambda - 2)^2 - 2 \right] |\lambda\mathbf{I} - \mathbf{A}|_{N-1}'^{linear} - (\lambda - 2)|\lambda\mathbf{I} - \mathbf{A}|_{N-2}'^{linear} + 2(-1)^{N+1} \quad (A7b)$$

where $|\lambda\mathbf{I} - \mathbf{A}|_n'^{linear} = |\lambda\mathbf{I} - \mathbf{A}|_n^{linear}/\lambda$

To compute the eigenvalues and eigenvectors of a ring chain, we can thus build on the corresponding known formulae for linear chains.¹¹¹ Indeed, according to eq A7a, we can propose that

$$\lambda - 2 = \exp(i\theta) + \exp(-i\theta) \quad (A8)$$

which (see eq A7) leads to the following general expression for the eigenvalues of a ring chain:

$$|\lambda\mathbf{I} - \mathbf{A}|_N^{ring} = c_1 \exp(iN\theta) + c_2 \exp(-iN\theta) + c_3 \quad (A9)$$

where c_1, c_2 , and c_3 are parameters to be determined. To this, one can resort to a procedure similar to that employed for a

linear chain.¹¹¹ Alternatively, and expediently, one can make use of the following relations:

$$\begin{aligned} |\lambda\mathbf{I} - \mathbf{A}|_3^{ring} &= \exp(i3\theta) + \exp(-i3\theta) + 2 \\ |\lambda\mathbf{I} - \mathbf{A}|_4^{ring} &= \exp(i4\theta) + \exp(-i4\theta) - 2 \\ |\lambda\mathbf{I} - \mathbf{A}|_5^{ring} &= \exp(i5\theta) + \exp(-i5\theta) + 2 \\ |\lambda\mathbf{I} - \mathbf{A}|_6^{ring} &= \exp(i6\theta) + \exp(-i6\theta) - 2 \\ &\vdots \end{aligned} \quad (\text{A10})$$

(obtained by inserting eq A8 into eq A7). By directly comparing then eqs A9 and A10 we find that $c_1 = 1$, $c_2 = 1$, and $c_3 = 2(-1)^{N+1}$. Equation A9 can therefore be re-expressed as

$$\begin{aligned} |\lambda\mathbf{I} - \mathbf{A}|_N^{ring} &= \exp(iN\theta) + \exp(-iN\theta) + 2(-1)^{N+1} \\ &= 2 \cos(N\theta) + 2(-1)^{N+1} \end{aligned} \quad (\text{A11})$$

To satisfy then $|\lambda\mathbf{I} - \mathbf{A}|_N^{ring} = 0$, the following relation must be imposed:

$$N\theta = (N+p)\pi \quad \text{for } p = 0, 2, 4, 6, \dots, N \quad (\text{A12a})$$

or, equivalently

$$\theta = \pi + \frac{p\pi}{N} \quad \text{for } p = 0, 2, 4, 6, \dots, N \quad (\text{A12b})$$

By substituting eq A12b into A8 we see that we can determine the eigenvalue that corresponds to the p -mode through:

$$\begin{aligned} \lambda_p - 2 &= 2 \cos\left(\pi + \frac{p\pi}{N}\right) = -2 \cos\left(\frac{p\pi}{N}\right) \quad \text{for} \\ p &= 0, 2, 4, 6, \dots, N \end{aligned} \quad (\text{A13})$$

from which we find the following final expression for all eigenvalues for an N -bead ring chain:

$$\begin{aligned} \lambda_p &= 2 - 2 \cos\left(\frac{p\pi}{N}\right) = 4 \sin^2\left(\frac{p\pi}{2N}\right) \quad \text{for} \\ p &= 0, 2, 4, 6, \dots, N \end{aligned} \quad (\text{A14})$$

This form is exactly the same as for the linear chain of the same length, but with the understanding that only even p modes survive in the case of rings.

To compute the corresponding eigenvectors $\xi_p = [\xi_{p1}, \xi_{p2}, \xi_{p3}, \dots, \xi_{pN}]^T$ we resort to the relation $(\lambda\mathbf{I} - \mathbf{A}) \cdot \xi_p = \mathbf{0}$ from which the following set of linear equations is obtained:¹¹¹

$$\begin{aligned} (\lambda_p - 2)\xi_{p1} + \xi_{p2} &= 0 \\ \xi_{p1} + (\lambda_p - 2)\xi_{p2} + \xi_{p3} &= 0 \\ \xi_{p2} + (\lambda_p - 2)\xi_{p3} + \xi_{p4} &= 0 \\ &\vdots \\ \xi_{p(N-3)} + (\lambda_p - 2)\xi_{p(N-2)} + \xi_{p(N-1)} &= 0 \\ \xi_{p(N-2)} + (\lambda_p - 2)\xi_{p(N-1)} &= 0 \end{aligned} \quad (\text{A15})$$

These can be described by the following recursive relation:

$$\begin{aligned} \xi_{p(n-1)} + \xi_{p(n+1)} &= (2 - \lambda_p)\xi_{pn} \quad \text{for} \\ n &= 2, 3, \dots, N-1 \end{aligned} \quad (\text{A16})$$

with the following boundary conditions for $n = 1$ and $n = N$:

$$(\lambda_p - 2)\xi_{p1} + \xi_{p2} + \xi_{pN} = 0 \quad (\text{A17a})$$

$$\xi_{p1} + \xi_{p(N-1)} + (\lambda_p - 2)\xi_{pN} = 0 \quad (\text{A17b})$$

Substituting then eq A14 into eq A16 we find

$$\begin{aligned} \xi_{p(n-1)} + \xi_{p(n+1)} &= \left[2 - 4 \sin^2\left(\frac{p\pi}{2N}\right) \right] \xi_{pn} \\ &= \left[\exp\left(\frac{ip\pi}{N}\right) + \exp\left(-\frac{ip\pi}{N}\right) \right] \xi_{pn} \end{aligned} \quad (\text{A18})$$

whose solution can be written as

$$\xi_{pn} = b_1 \exp\left(\frac{ipn\pi}{N}\right) + b_2 \exp\left(-\frac{ipn\pi}{N}\right) \quad (\text{A19})$$

Applying eq A19 to the boundary conditions (eq A17) yields $b_1 = -b_2$. Thus, eq A16 becomes

$$\begin{aligned} \xi_{pn} &= b_1 \left[\exp\left(\frac{ipn\pi}{N}\right) - \exp\left(-\frac{ipn\pi}{N}\right) \right] \\ &= b_1(2i) \sin\left(\frac{pn\pi}{N}\right) \end{aligned} \quad (\text{A20})$$

With the help of the normalization condition that

$$\sum_{n=1}^N \xi_{pn} \xi_{pn}^* = 1$$

(the superscript * denotes the complex conjugate), b_1 is found to be equal to $1/\sqrt{2N}$. We thus arrive at the following desired expression for the eigenvector that corresponds to the p th eigenvalue:

$$\xi_{pn} = \sqrt{\frac{2}{N}} \sin\left(\frac{pn\pi}{N}\right) \quad \text{for } p = 2, 4, 6, \dots, N-2 \quad (\text{A21})$$

with the understanding that, except for the 0th eigenvalue which is equal to zero (i.e., $\lambda_0 = 0$) and the last eigenvalue for $p = N$ (in case N is an even number) which have a multiplicity of 1, all the others have a multiplicity of 2 for ring chains thus giving rise to two independent eigenvectors. And eq A21 gives only one of these two eigenvectors for each eigenvalue.

Note Added after ASAP Publication. This article posted ASAP on November 11, 2010. The sentence above equation 31 and equations 31, 32, 33, and 34 have been revised. The correct version posted on November 19, 2010.

References and Notes

- (1) Ferry, J. D. *Viscoelastic Properties of Polymers*; J. Wiley & Sons: New York, 1980.
- (2) Bird, R. B.; Armstrong, R. C.; Hassanger, O. *Dynamics of Polymeric Liquids*, 2nd ed.; John Wiley and Sons, Inc.: New York, 1987; Vols. 1 and 2.
- (3) Rubinstein, M.; Colby, R. H. *Polymer Physics*; Oxford University Press: New York, 2003.
- (4) Larson, R. G. *The Structure and Rheology of Complex Fluids*; Oxford University Press: New York, 1999.

- (5) Voit, B. I.; Lederer, A. *Chem. Rev.* **2009**, *109*, 5924.
 (6) Carlmark, A.; Hawker, C.; Hult, A.; Malkoch, M. *Chem. Soc. Rev.* **2009**, *38*, 352.
 (7) Watanabe, H.; Matsumiya, Y.; van Ruymbeke, E.; Vlassopoulos, D.; Hadjichristidis, N. *Macromolecules* **2008**, *41*, 6110.
 (8) DeGennes, P. J. *J. Chem. Phys.* **1971**, *55*, 572.
 (9) Doi, M.; Edwards, S. F. *The Theory of Polymer Dynamics*; Clarendon Press: Oxford, England, 1986.
 (10) Doi, M.; Edwards, S. F. *J. Chem. Soc. Faraday Trans. 2* **1978**, *74*, 1789. Doi, M.; Edwards, S. F. *J. Chem. Soc. Faraday Trans. 2* **1978**, *74*, 1802. Doi, M.; Edwards, S. F. *J. Chem. Soc. Faraday Trans. 2* **1978**, *74*, 1818. Doi, M.; Edwards, S. F. *J. Chem. Soc. Faraday Trans. 2* **1979**, *75*, 38.
 (11) McLeish, T. C. B. *Adv. Phys.* **2002**, *51*, 1379.
 (12) Watanabe, H. *Prog. Polym. Sci.* **1999**, *24*, 1253.
 (13) Graessley, W. W. *Adv. Polym. Sci.* **1974**, *16*, 1.
 (14) McLeish, T. C. B. *Nat. Mater.* **2008**, *7*, 933.
 (15) Klein, J. *Macromolecules* **1986**, *19*, 105.
 (16) Kramers, H. A. *J. Chem. Phys.* **1946**, *14*, 415.
 (17) Zimm, B. H.; Stockmayer, W. H. *J. Chem. Phys.* **1949**, *17*, 1301.
 (18) Casassa, E. F. *J. Polym. Sci., Part A: Polym. Chem. Ed.* **1965**, *3*, 605.
 (19) Bloomfield, V.; Zimm, B. H. *J. Chem. Phys.* **1966**, *44*, 315.
 (20) Fukatsu, M.; Kurata, M. *J. Chem. Phys.* **1966**, *44*, 4539.
 (21) Rouse, P. E. *J. Chem. Phys.* **1953**, *21*, 1272.
 (22) Zimm, B. H. *J. Chem. Phys.* **1956**, *24*, 269.
 (23) Watanabe, H.; Inoue, T.; Matsumiya, Y. *Macromolecules* **2006**, *39*, 5419.
 (24) Arrighi, V.; Gagliardi, S.; Dagger, A. C.; Semlyen, J. A.; Higgins, J. S.; Shenton, M. *J. Macromolecules* **2004**, *37*, 8057.
 (25) Gagliardi, S.; Arrighi, V.; Dagger, A.; Semlyen, A. *J. Appl. Phys. A: Mater. Sci. Process.* **2002**, *74*, S469.
 (26) Suzuki, J.; Takano, A.; Deguchi, T.; Matsushita, Y. *J. Chem. Phys.* **2009**, *131*, 144902.
 (27) Hur, K.; Winkler, R. G.; Yoon, D. Y. *Macromolecules* **2006**, *39*, 3975.
 (28) Brown, S.; Szamel, G. *J. Chem. Phys.* **1998**, *108*, 4705.
 (29) Muller, M.; Wittmer, J. P.; Cates, M. E. *Phys. Rev. E* **1996**, *53*, 5063.
 (30) Muller, M.; Wittmer, J. P.; Cates, M. E. *Phys. Rev. E* **2000**, *61*, 4078.
 (31) Brown, S.; Lenczycki, T.; Szamel, G. *Phys. Rev. E* **2001**, *63*, 052801.
 (32) Geyler, S.; Pakula, T. *Makromol. Chem. Rapid Commun.* **1988**, *9*, 617.
 (33) Iyer, B. V. S.; Lele, A. K.; Shanbhag, S. *Macromolecules* **2007**, *40*, 5995.
 (34) Deutsch, J. M. *Phys. Rev. E* **1999**, *59*, R2539.
 (35) Khokhlov, A. R.; Nechaev, S. L. *Phys. Lett.* **1985**, *112A*, 156.
 (36) Rubinstein, M. *Phys. Rev. Lett.* **1986**, *57*, 3023.
 (37) Obukhov, S. P.; Rubinstein, M.; Duke, T. *Phys. Rev. Lett.* **1994**, *73*, 1263.
 (38) Kapnistos, M.; Lang, M.; Vlassopoulos, D.; Pyckhout-Hintzen, W.; Richter, D.; Cho, D.; Chang, T.; Rubinstein, M. *Nat. Mater.* **2008**, *7*, 997.
 (39) Roovers, J. *Macromolecules* **1985**, *18*, 1359.
 (40) Roovers, J. *Macromolecules* **1988**, *21*, 1517.
 (41) McKenna, G. B.; Plazek, D. *J. Polym. Commun.* **1986**, *27*, 304.
 (42) McKenna, G. B.; Hostetter, B. J.; Hadjichristidis, N.; Fetters, L. J.; Plazek, D. *J. Macromolecules* **1989**, *22*, 1834.
 (43) Mills, P. J.; Mayer, J. W.; Kramer, E. J.; Hadzioannou, G.; Lutz, P.; Strazielle, C.; Rempp, P.; Kovacs, A. *J. Macromolecules* **1987**, *20*, 513.
 (44) Tead, S. F.; Kramer, E. J.; Hadzioannou, G.; Antonietti, M.; Sillescu, H.; Lutz, P.; Strazielle, C. *Macromolecules* **1992**, *25*, 3942.
 (45) Orrah, D. J.; Semlyen, J. A.; Rossmurphy, S. B. *Polymer* **1988**, *29*, 1455.
 (46) Cosgrove, T.; Turner, M. J.; Griffiths, P. C.; Hollingshurst, J.; Shenton, M. J.; Semlyen, J. A. *Polymer* **1996**, *37*, 1535.
 (47) Ozisik, R.; von Meerwall, E. D.; Mattice, W. L. *Polymer* **2002**, *43*, 629.
 (48) von Meerwall, E.; Ozisik, R.; Mattice, W. L.; Pfister, P. M. *J. Chem. Phys.* **2003**, *118*, 3867.
 (49) Nam, S.; Leisen, J.; Breedveld, V.; Beckham, H. W. *Polymer* **2008**, *49*, 5467.
 (50) Nam, S.; Leisen, J.; Breedveld, V.; Beckham, H. W. *Macromolecules* **2009**, *42*, 3121.
 (51) Dodgson, K.; Semlyen, J. A. *Polymer* **1977**, *18*, 1256.
 (52) Dodgson, K.; Bannister, D. J.; Semlyen, J. A. *Polymer* **1980**, *21*, 663.
 (53) Edwards, C. J. C.; Richards, R. W.; Stepto, R. F. T.; Dodgson, K.; Higgins, J. S.; Semlyen, J. A. *Polymer* **1984**, *25*, 365.
 (54) Higgins, J. S.; Dodgson, K.; Semlyen, J. A. *Polymer* **1979**, *18*, 553.
 (55) Higgins, J. S.; Ma, K.; Nicholson, L. K.; Hayter, J. B.; Dodgson, K.; Semlyen, J. A. *Polymer* **1983**, *24*, 793.
 (56) Hild, G.; Strazielle, C.; Rempp, P. *Eur. Polym. J.* **1983**, *19*, 721.
 (57) Roovers, J. *J. Polym. Sci., Part B: Polym. Phys.* **1985**, *23*, 1117.
 (58) Lutz, P.; McKenna, G. B.; Rempp, P. *Makromol. Chem. Rapid Commun.* **1986**, *7*, 599.
 (59) McKenna, G. B.; Hadzioannou, G.; Lutz, P.; Hild, G.; Strazielle, C.; Straupe, C.; Rempp, P.; Kovacs, A. *J. Macromolecules* **1987**, *20*, 498.
 (60) Kawaguchi, D.; Masuoka, K.; Takano, A.; Tanaka, K.; Nagamura, T.; Torikai, N.; Dalgleish, R. M.; Langridge, S.; Matsushita, Y. *Macromolecules* **2006**, *39*, 5180.
 (61) Robertson, R. M.; Smith, D. E. *Proc. Natl. Acad. Sci. U.S.A.* **2007**, *104*, 4824.
 (62) (a) Lee, H. C.; Lee, H.; Lee, W.; Chang, T.; Roovers, J. *Macromolecules* **2000**, *33*, 8119. (b) Lee, W.; Lee, H.; Lee, H. C.; Cho, D.; Chang, T.; Gorbunov, A. A.; Roovers, J. *Macromolecules* **2002**, *35*, 529.
 (63) Cho, D.; Masuoka, K.; Koguchi, K.; Asari, T.; Kawaguchi, D.; Takano, A.; Matsushita, Y. *Polymer J* **2005**, *37*, 506.
 (64) Vettorel, T.; Grosberg, A. Y.; Kremer, K. *Phys. Biol.* **2009**, *6*, 025013.
 (65) Vettorel, T.; Reigh, S. Y.; Yoon, D. Y.; Kremer, K. *Macromol. Rapid Commun.* **2009**, *30*, 345.
 (66) Jang, S. S.; Cagin, T.; Goddard, W. A. *J. Chem. Phys.* **2003**, *119*, 1843.
 (67) Brown, S.; Szamel, G. *J. Chem. Phys.* **1998**, *109*, 6184.
 (68) Cates, M. E.; Deutsch, J. M. *J. Phys. (Paris)* **1986**, *47*, 2121.
 (69) Doruker, P.; Mattice, W. L. *J. Phys. Chem. B* **1999**, *103*, 178.
 (70) Fu, C. L.; Ouyang, W.; Sun, Z. Y.; An, L. *J. Chem. Phys.* **2007**, *127*, 044903.
 (71) Brereton, M. G.; Vilgis, T. A. *J. Phys. A: Math. Theor.* **1995**, *28*, 1149.
 (72) Suzuki, J.; Takano, A.; Matsushita, Y. *J. Chem. Phys.* **2008**, *129*, 034903.
 (73) Subramanian, G.; Shanbhag, S. *Macromolecules* **2008**, *41*, 7239.
 (74) Subramanian, G.; Shanbhag, S. *Phys. Rev. E* **2008**, *77*, 011801.
 (75) Iyer, B. V. S.; Shanbhag, S.; Juvekar, V. A.; Lele, A. K. *J. Polym. Sci., Part B: Polym. Phys.* **2008**, *46*, 2370.
 (76) Karayiannis, N. C.; Mavrantzas, V. G. *Macromolecules* **2005**, *38*, 8583.
 (77) Nath, S. K.; Khare, R. *J. Chem. Phys.* **2001**, *115*, 10837.
 (78) Van der Ploeg, P.; Berendsen, H. J. C. *J. Chem. Phys.* **1982**, *76*, 3271.
 (79) Toxvaerd, S. *J. Chem. Phys.* **1997**, *107*, 5197.
 (80) Martin, M. G.; Siepmann, J. I. *J. Phys. Chem. B* **1998**, *102*, 2569.
 (81) Materials Studio, Accelrys Software Inc.: San Diego CA.
 (82) Nosé, S. *Mol. Phys.* **1984**, *52*, 255.
 (83) Nosé, S. *J. Chem. Phys.* **1984**, *81*, 511.
 (84) Nosé, S. *Prog. Theor. Phys. Suppl.* **1991**, *103*, 1.
 (85) Hoover, W. G. *Phys. Rev. A* **1985**, *31*, 1695.
 (86) Martyna, G. J.; Tuckerman, M. E.; Tobias, D. J.; Klein, M. L. *Mol. Phys.* **1996**, *87*, 1117.
 (87) Plimpton, S. www.sandia.gov/~sjplimp/lammps.html.
 (88) Plimpton, S. *J. J. Comput. Phys.* **1995**, *117*, 1.
 (89) Takano, A.; Kushida, Y.; Ohta, K.; Masuoka, K.; Matsushita, Y. *Polymer* **2009**, *50*, 1300.
 (90) Edwards, C. J. C.; Rigby, D.; Stepto, R. F. T.; Dodgson, K.; Semlyen, J. A. *Polymer* **1983**, *24*, 391.
 (91) Lohse, D. J. *J. Macromol. Sci., Part C: Polym. Rev.* **2005**, *C45*, 289.
 (92) Tsouli, G.; Harmandaris, V. A.; Mavrantzas, V. G. *Macromol. Theory and Simul.* **2006**, *15*, 381.
 (93) Tsouli, G.; Mavrantzas, V. G.; Makrodimitri, Z. A.; Economou, I. G.; Gani, R. *Macromolecules* **2008**, *41*, 6228.
 (94) Olabisi, O.; Simha, R. *Macromolecules* **1975**, *8*, 206.
 (95) Gestoso, P.; Karayiannis, N. C. *J. Phys. Chem. B* **2008**, *112*, 5646.
 (96) Simha, R.; Wilson, P. S. *Macromolecules* **1973**, *6*, 908.
 (97) Wilson, P. S.; Simha, R. *Macromolecules* **1973**, *6*, 902.
 (98) Mavrantzas, V. G.; Boone, T. D.; Zervopoulou, E.; Theodorou, D. N. *Macromolecules* **1999**, *32*, 5072.

- (99) Harmandaris, V. A.; Mavrntzas, V. G.; Theodorou, D. N. *Macromolecules* **1998**, *31*, 7934.
- (100) Šolc, K.; Stockmayer, W. H. *J. Chem. Phys.* **1971**, *54*, 2756.
- (101) Theodorou, D. N.; Suter, U. W. *Macromolecules* **1985**, *18*, 1206.
- (102) Tsolou, G.; Mavrntzas, V. G.; Theodorou, D. N. *Macromolecules* **2005**, *38*, 1478.
- (103) Smith, G. D.; Paul, W.; Monkenbusch, M.; Richter, D. *Chem. Phys.* **2000**, *261*, 61.
- (104) Smith, G. D.; Paul, W.; Monkenbusch, M.; Richter, D. *J. Chem. Phys.* **2001**, *114*, 4285.
- (105) Harmandaris, V. A.; Mavrntzas, V. G.; Theodorou, D. N.; Kröger, M.; Ramírez, J.; Öttinger, H. C.; Vlassopoulos, D. *Macromolecules* **2003**, *36*, 1376.
- (106) Tsolou, G.; Harmandaris, V. A.; Mavrntzas, V. G. *J. Non-Newtonian Fluid Mech.* **2008**, *152*, 184.
- (107) Stephanou, P. S.; Baig, C.; Tsolou, G.; Mavrntzas, V. G.; Kröger, M. *J. Chem. Phys.* **2010**, *132*, 124904.
- (108) Pearson, D. S.; Ver Strate, G.; von Meerwall, E.; Schilling, F. C. *Macromolecules* **1987**, *20*, 1133.
- (109) Pearson, D. S.; Fetters, L. J.; Graessley, W. W.; Strate, G.; von Meerwall, V. E. *Macromolecules* **1994**, *27*, 711.
- (110) Arfken, G. B.; Weber, H. J. *Mathematical Methods for Physicists*, 5th ed.; Academic Press: San Diego, CA, 2001.
- (111) Lin, Y.-H. *Polymer Viscoelasticity: Basics, Molecular Theories, and Experiments*; World Scientific Publishing: Singapore, 2003.